



HAL
open science

Impact of dust and temperature on primary productivity in Late Miocene oceans

Anta-clarisse Sarr, Yannick Donnadiou, Anthony Gramoullé, Baptiste Suchéras-Marx, Quentin Pillot

► **To cite this version:**

Anta-clarisse Sarr, Yannick Donnadiou, Anthony Gramoullé, Baptiste Suchéras-Marx, Quentin Pillot. Impact of dust and temperature on primary productivity in Late Miocene oceans. 2023. hal-04363317

HAL Id: hal-04363317

<https://hal.science/hal-04363317>

Preprint submitted on 24 Dec 2023

HAL is a multi-disciplinary open access archive for the deposit and dissemination of scientific research documents, whether they are published or not. The documents may come from teaching and research institutions in France or abroad, or from public or private research centers.

L'archive ouverte pluridisciplinaire **HAL**, est destinée au dépôt et à la diffusion de documents scientifiques de niveau recherche, publiés ou non, émanant des établissements d'enseignement et de recherche français ou étrangers, des laboratoires publics ou privés.



Distributed under a Creative Commons Attribution - NonCommercial - ShareAlike 4.0 International License

1

2

Impact of dust and temperature on primary productivity in Late Miocene oceans

3

4

Pillot Q.¹, Sarr A-C.², Donnadieu Y.¹, Gramoullé A.¹ and Suchéras-Marx B.¹

5

¹CEREGE, Aix Marseille Univ, CNRS, IRD, INRAE, France.

6

²Univ. Grenoble Alpes, Univ. Savoie Mont Blanc, CNRS, IRD, Univ. Gustave Eiffel, ISTerre, 38000

7

Grenoble, France

8

Key Points:

9

10

11

12

13

- Increased dust deposition increases primary productivity in the Miocene oceans.
- Cooling, linked to the decrease in atmospheric pCO₂ concentration, leads to a reduction in primary productivity in the Miocene oceans.
- Global aridification could have contributed to the onset of the Late Miocene Biogenic Bloom while cooling might have triggered its decline.

Corresponding author: Pillot Q., pillot@cerege.fr

Abstract

Most of the primary productivity in the ocean comes from phytoplankton, and is impacted, among other things, by the amount of nutrients available, as well as by temperature. The Late Miocene and Pliocene were marked by global aridification, linked to the emergence of the large deserts, likely increasing the input of dust and thus nutrients into the ocean. There was also a global decrease in temperature during this period, linked to a decline in atmospheric CO₂ concentration. The objective of this study is to quantify the impact of dust and pCO₂ levels on primary productivity in the oceans under Late Miocene boundary conditions. New simulations were performed with the coupled ocean-atmosphere model IPSL-CM5A2 and its marine biogeochemistry component PISCES with a Late Miocene paleogeography. Our results show that an increase in dust input produces a quasi-generalized increase in primary productivity, associated with a decrease in nutrient limitation. This increase in productivity also leads to nutrient deficits in some areas. The decrease in pCO₂ levels and the associated lower water temperatures lead to a reduction in primary productivity. This decrease is mainly due to a reduction in the supply of nutrients resulting from less intense remineralization. In addition, our results show that change in carbon export resulting from change in dust input and temperature are highly heterogeneous spatially. Simulations combined with sedimentary data suggesting a link between aridification, cooling and the Biogenic Bloom of the Late Miocene and Pliocene.

1 Introduction

Phytoplanktons are responsible for most of the primary productivity in present-day oceans (Field et al., 1998). Their development depends on temperature conditions, light that limits their proliferation to surface layers and the supply of nutrients (Field et al., 1998; Balch, 2004). Among these nutrients, it is mainly the available quantity of nitrogen, iron and sometimes phosphorus that limits phytoplankton growth (C. M. Moore et al., 2013). These nutrients can come from the subsurface waters, such as in mixing zones and upwelling regions (Sarmiento et al., 2004), or from the continents via rivers (Sharples et al., 2017) and atmospheric dust (T. Jickells & Moore, 2015) transported by winds from deserts and arid source zones in particular (N. M. Mahowald et al., 2005; Hooper et al., 2019). Brief and localized episodes of dust deposition can even cause productivity blooms in some ocean areas, such as in the Yellow Sea (Shi et al., 2012), the South Atlantic (Dansie et al., 2022) and the Arabian Sea (Banerjee & Prasanna Kumar, 2014). As previously mentioned, ocean temperature is also a parameter that can influence the development of phytoplankton. This happens because temperature modulates bacteriological activity responsible for the degradation of organic matter (called remineralization or respiration), which in turn, is a source of nutrients for primary productivity (del Giorgio & Duarte, 2002). This bacteriological activity, and therefore the supply of nutrients through remineralization, increases as water temperature rises (López-Urrutia et al., 2006; Bendtsen et al., 2015). Increase in surface water temperature can on the other hand also lead to stratification of the water column, slowing down the supply of nutrients from the subsurface, balancing the remineralization effect (Behrenfeld et al., 2006).

Both the supply of dust to the ocean and temperature are parameters that have fluctuated throughout the Earth's history. During the Late Miocene (~ 11-5 Ma) and Pliocene (~ 5-3 Ma) periods, the climate became colder and drier, transitioning toward the one we know today (Steinhorsdottir et al., 2021). The significant drop in atmospheric pCO₂ at this time (from around 600 ppm in the mid-Miocene to around 400 ppm in the early Pliocene, Rae et al. (2021), Sosdian et al. (2018), de la Vega et al. (2020)) is probably responsible for this temperature decrease (Martinot et al., 2022; Hossain et al., 2023). Global cooling is associated with an increase in the latitudinal gradient of ocean surface temperature (Herbert et al., 2016; Martinot et al., 2022; Lohmann et al., 2022). The strengthening of this gradient leads to greater air mass movement in the atmosphere, causing Walker and Hadley cells

65 and trade winds intensification (Kamae et al., 2011). Vegetation has also changed signif-
66 icantly, notably with the proliferation of plants using C₄ photosynthesis (i.e. steppes) to
67 the detriment of those using C₃ photosynthesis (i.e. forests, Cerling et al. (1997), Feakins
68 et al. (2013), Tauxe and Feakins (2020)). This proliferation, thought to be linked to global
69 aridification (Pound et al., 2012; Sepulchre et al., 2006), began around 10 Ma ago in tropical
70 Africa (Polissar et al., 2019) and around 3.5 Ma ago in Australia (Andrae et al., 2018). In
71 some places, vegetation is disappearing and replaced by major modern deserts (Schuster et
72 al., 2006; Fujioka et al., 2009; Pound et al., 2012; Z. Zhang et al., 2014; Rech et al., 2019;
73 Abell et al., 2020; Crocker et al., 2022). Reduced vegetation cover, due to arid climates,
74 increases wind erosion and therefore the input of dust into the atmosphere (Hovan, 1995).

75 Such cooling and apparent aridification should have impacted primary productivity,
76 though this has never been explicitly quantified. During the Late Miocene, productivity has
77 considerably varied, with one major increase that lasted for several million years. This high
78 productivity event, known as the Late Miocene Biogenic Bloom (LMBB), is characterized by
79 high rates of calcite accumulation from calcareous nannofossils and planktonic foraminifera,
80 and opals from diatoms and radiolarians (Farrell et al., 1995; Dickens & Owen, 1999; Grant
81 & Dickens, 2002; Diester-Haass et al., 2005; Lyle & Baldauf, 2015; Drury et al., 2021;
82 Gastaldello et al., 2023). Evidence of LMBB has been found in every oceanic basins. In
83 the Pacific Ocean, studies suggest the presence of LMBB in the equatorial part of the basin
84 (Farrell et al., 1995; Lyle & Baldauf, 2015; Lyle et al., 2019), in the southwestern ocean
85 (Grant & Dickens, 2002; Gastaldello et al., 2023) and in the South China Sea (L. Zhang
86 et al., 2009). In the Atlantic Ocean, there are traces of the event both in the northern
87 (Diester-Haass et al., 2005), and southern basins (Hermoyian & Owen, 2001; Diester-Haass
88 et al., 2005; Drury et al., 2021). LMBB has also been found in Indian Ocean sediments
89 (Dickens & Owen, 1999; Hermoyian & Owen, 2001; Lübbers et al., 2019; Bolton et al.,
90 2022). Although recorded in different oceanic basins, the LMBB appears to have a very
91 heterogeneous spatial distribution, and many drill sites show no record of the event (Pillot
92 et al., 2023; Lyu et al., 2023). A compilation of LMBB data has suggested a start date
93 between 7 and 8 Ma and an end date between 2 and 3 Ma, with a maximum between 6 and
94 7 Ma (Pillot et al., 2023). However, studies show that the LMBB could have begun earlier,
95 around 11-12 Ma (L. Zhang et al., 2009; Lübbers et al., 2019) and concluded earlier, around
96 4.5 Ma (Karatsolis et al., 2022). To explain the cause of this event, various hypotheses,
97 which are not mutually incompatible, have been advanced in the literature. Some suggest
98 that the increase in productivity could be the result of an increase in the supply of nutrients
99 from the continents to the oceans (Pisias et al., 1995; Filippelli, 1997; Hermoyian & Owen,
100 2001; Gupta et al., 2004). This event could also result from a redistribution of nutrients in
101 the ocean through a reorganization of ocean circulation (Dickens & Owen, 1999; Farrell et
102 al., 1995; Pisias et al., 1995) or through a generalized increase in upwelling systems (Pillot
103 et al., 2023). The cause of the end of the LMBB has been less discussed in the literature.
104 Farrell et al. (1995) suggest that the definitive closure of the Central American seaway could
105 have triggered the end of the event by preventing water exchange between the Atlantic and
106 Pacific oceans. More recently, Karatsolis et al. (2022) propose that the hydrological cycle –
107 and therefore the supply of nutrients via rivers – was slowed down by a decrease in insolation
108 due to a particular orbital configuration.

109 Although several studies already investigated the link between pCO₂, dust and primary
110 productivity in a present-day context (Dutkiewicz et al., 2005; Tagliabue et al., 2008,
111 2009; Steinacher et al., 2010), this is not the case in a geographical and climatic con-
112 text corresponding to the Late Miocene, preventing the understanding of mechanisms at
113 play in the change of primary productivity for this time period. In this study we use a
114 coupled ocean-atmosphere model including a marine biogeochemistry component with Late
115 Miocene boundary conditions to investigate how dust deposition and cooling affects primary
116 production. We focus on the evolution of primary productivity in response to (1) increas-
117 ing atmospheric dust deposition in the oceans and (2) decreasing CO₂ partial pressure and

118 associated global cooling. Our results are then discussed in the context of the LMBB (to
 119 propose a hypothesis to explain the onset and the end of this event).

120 2 Methods

121 2.1 Model

122 In this study, we used the IPSL-CM5A2 Earth System Model (Sepulchre et al., 2020)
 123 to perform the simulations. This model is an updated version of the IPSL-CM5A-LR model
 124 (Dufresne et al., 2013), with bias corrections and reduced computation times that enable
 125 to perform multimillennial simulations typical of paleoclimate studies. It is composed of
 126 the ocean model NEMO (Madec, 2016), the land surface and vegetation model ORCHIDEE
 127 (Krinner et al., 2005) and the atmospheric model LMDz-5A (Hourdin et al., 2013). At-
 128 mospheric and ocean component are linked by the OASIS coupler (Valcke, 2013). The
 129 atmosphere model has a resolution of 96×96 or 3.75° in longitude and 1.875° in latitude
 130 over 39 vertical levels. The ocean grid has 31 vertical levels (varying in thickness from 10
 131 m near the surface to 500 m on the ocean floor) and a horizontal resolution of 2° by 2° ,
 132 decreasing to 0.5° near the equator. More details on the parameterization of this model can
 133 be found in Sepulchre et al. (2020). In addition to ocean-atmosphere simulations we also
 134 use the offline version of PISCES-v2 model (Aumont et al., 2015), which is a marine biogeo-
 135 chemical model that simulates the main biogeochemical cycles as well as marine ecosystems
 136 (including diatoms, nanophytoplankton, microzooplankton and mesozooplankton). In this
 137 model, phytoplankton growth is limited by nutrient availability (phosphorus, nitrogen, iron
 138 and silica), light and water temperature (see Aumont et al. (2015), for detailed equations).
 139 These models have already been used to study the Miocene climate (Martinot et al., 2022;
 140 Sarr et al., 2022; Pillot et al., 2022; Burls et al., 2021; Tardif et al., 2023).

141 2.2 Experiments and Boundary Conditions

142 We used climatic fields from three Late Miocene ocean-atmosphere coupled simulations
 143 with different $p\text{CO}_2$ (300ppm, 420ppm and 560ppm from Sarr et al. (2022) and Martinot et
 144 al. (2022)) as inputs for the offline version of the PISCES-v2 model. The ocean dynamics
 145 for each simulation are described in the the following subsection. These simulations have
 146 been shown to mimic the amplitude of temperature decline during the Late Miocene, when
 147 compared to SST records (Martinot et al., 2022). The SSTs from the Mio420Dust and
 148 Mio560Dust simulations are in good agreement with SST recorded around the early Late
 149 Miocene (8 Ma) (Martinot et al., 2022). The SSTs from the Mio300Dust simulation are too
 150 low compared with the late Late Miocene (6 Ma) record but they could correspond to more
 151 recent times (Martinot et al., 2022). We first performed three simulations with PISCES-v2
 152 as follow up of coupled simulations at 300 ppm, 420 ppm and 560 ppm mentioned above
 153 (Mio300Dust, Mio420Dust and Mio560Dust) that enabled us to look at the effect of temper-
 154 ature changes (Figure 1A) on primary productivity. In these simulations, atmospheric dust
 155 are set to pre-industrial values. The concentration of nutrients in the rivers was calibrated
 156 to the total runoff flux in order to maintain the modern total amount of nutrients transferred
 157 to the ocean. We then run three additional simulations at 420ppm : those one are forced
 158 with ocean fields identical to Mio420Dust but we varied the quantity of nutrients in atmo-
 159 spheric dust (iron, nitrogen and phosphorus) in order to test the effect of dust supply on
 160 primary productivity. The present-day concentration of each nutrients was divided by 2 in
 161 the Mio420Dust2 simulation, divided by 10 in the Mio420Dust10 simulation and divided by
 162 1,000 in the Mio420NoDust simulation. The concentrations for each simulation are shown
 163 in Table 1. In order to constrain the geographical distribution of dust, satellite observations
 164 were used to constrain the geographical distribution of dust (Figure 1B, Balkanski et al.
 165 (2004)). Each nutrient has a proportion of the total concentration and an ocean solubility
 166 value. For phosphorus, the total content is 750 ppm and the solubility is 10% (N. Mahowald
 167 et al., 2008). For iron, the proportion is 3.5% (T. D. Jickells et al., 2005) with a solubility

Table 1. Experimental design. PP: Primary productivity by Phytoplanktons. EXPC: Export of carbon particles. For phosphorus, the total content is 750 ppm and the solubility is 10% (N. Mahowald et al., 2008). For iron, the proportion is 3.5% (T. D. Jickells et al., 2005) with a solubility of 20%. Finally, silica is prescribed according to J. Moore et al. (2001) with a solubility of 7.5%

Simulation	CO ₂ (ppm)	Average SST (°C)	Iron from dust (Tg/yr)	Phosphorus from dust (Tg/yr)	Silice from dust (Tg/yr)	Average integrated PP (g/m ² /day)	Average EXPC at 100 m (g/m ² /day)
Mio420Dust	420	20.4	0.3312	0.03478	10.93	0.35	0.054
Mio420Dust2	420	20.4	0.1656	0.01739	5.465	0.34	0.051
Mio420Dust10	420	20.4	0.03314	0.003478	1.093	0.33	0.049
Mio420NoDust	420	20.4	0.0003539	0.00003486	0.01096	0.32	0.048
Mio300Dust	300	19.1	0.3312	0.03478	10.93	0.33	0.052
Mio560Dust	560	21.6	0.3312	0.03478	10.93	0.38	0.056

168 of 20%. Finally, silica is prescribed according to J. Moore et al. (2001) with a solubility of
 169 7.5%. For phosphorus and silica, deposition is limited to the first level of the ocean model
 170 (More details can be found in Aumont et al. (2015)). Coupled simulations have been run
 171 for 3,000 years, and the last 100 years have been averaged to provide an initial state for the
 172 PISCES simulations, which have also been run for 3,000 years. Model outputs presented
 173 here are averaged over the last 100 years of each simulation.

174 Our simulations were carried out with a Late Miocene paleogeography based on PlioMIP
 175 geography (Haywood et al. (2020), Figure 1C). Although close to present-day geography,
 176 some differences may significantly affect the global ocean circulation and hence nutrient dis-
 177 tribution. Those major differences include a closed Bering Seaway (Gladenkov & Gladenkov,
 178 2004) and an Australian continent located further south than at present-day (widening the
 179 Indonesian Throughflow that connects the Indian and Pacific Oceans, Kuhnt et al. (2004)),
 180 which might be responsible for a oceanic circulation different from present-day (Brierley &
 181 Fedorov, 2016; Tan et al., 2022). The ice-sheet cover on Greenland is also smaller (Bierman
 182 et al., 2016), which also implies a different circulation compared to the modern one in the
 183 Atlantic Ocean (Davini et al., 2015; Pillot et al., 2022).

184 2.3 Ocean dynamics of input simulations

185 Ocean circulation is very similar in the Mio300Dust, Mio420Dust and Mio560Dust
 186 coupled simulations (Figure 2). The meridional overturning circulation is composed of two
 187 main cells: North Atlantic Deep Water (NADW, in blue in Figure 2A) and Antarctic Bottom
 188 Water (AABW, in red in Figure 2A). The structure of the two cells is very similar between
 189 simulations, but they are slightly weaker in the Mio560Dust simulation (Figure 2A). The
 190 formation of NADW happens during winter, and the sinking zones are located between 50°
 191 and 75° N (Figure 2B). The most important zone is located in the Labrador Sea, between 50
 192 and 60°N, with a mixed layer depth exceeding 1,800 m depth. The location of the sinking
 193 zones are the same in all three simulations. However, in the Mio560Dust simulation, the
 194 sinking zone in the Labrador Sea is slightly larger, in detriment of the northern zones (Figure
 195 2B). In the Southern Ocean, the sinking zone leading to AABW is located in the Weddell
 196 Sea, between 60 and 70°S, for the three simulations (Figure 2C). The depth of the mixed
 197 layer in this zone reaches 2,000 m for the Mio300Dust and Mio420Dust simulations, and
 198 exceeds 2,500 m for the Mio560Dust simulation. However, the AABW has a lower flow rate
 199 in the Mio560Dust simulation, reaching 7 Sv at the center of the cell, compared to 10 Sv for

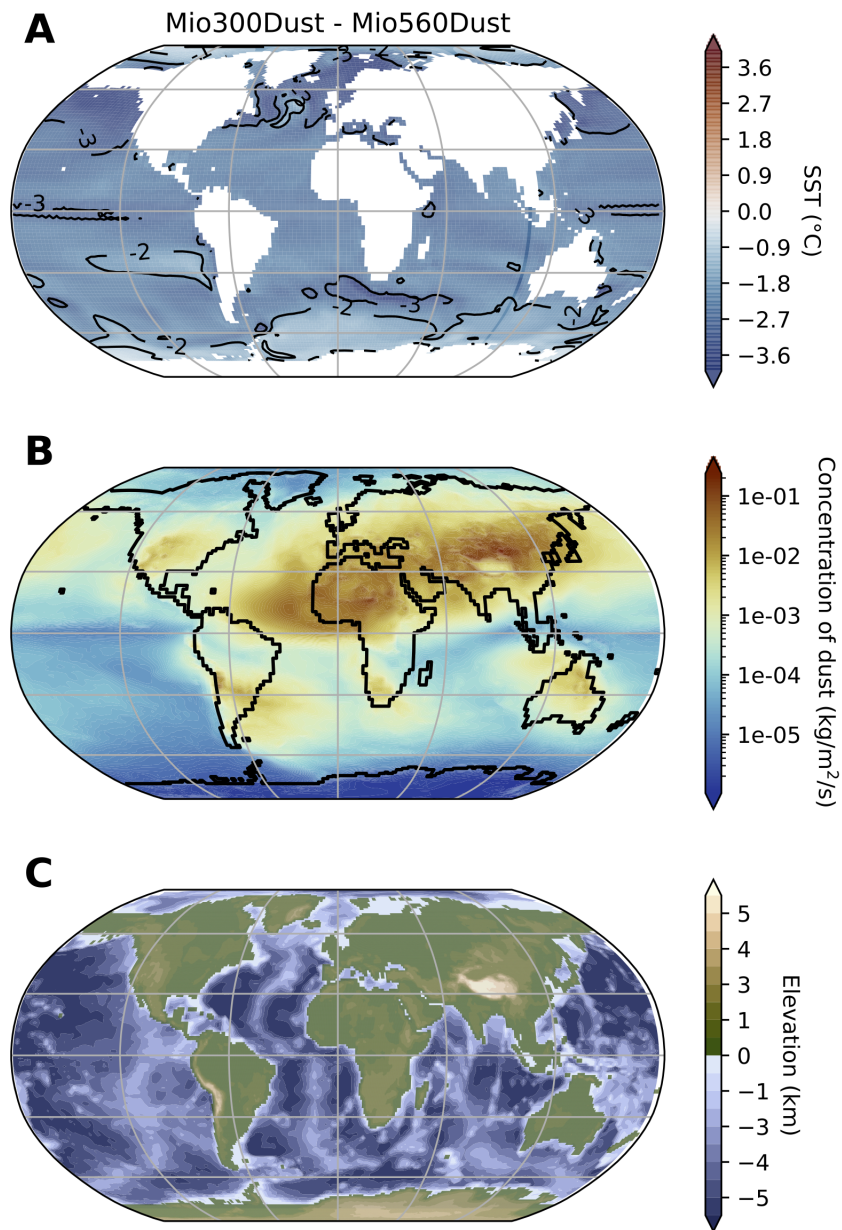


Figure 1. A: Difference in SST (°C) between the Mio300Dust and Mio560Dust simulations averaged over the year (modified from Martinot et al. (2022)). B: Atmospheric dust concentration averaged over the year (kg/m²/s) for the Mio300Dust, Mio420Dust and Mio560Dust simulations. C: Paleogeography used for the simulations (km).

the Mio300Dust and Mio420Dust simulations (Figure 2A). At the surface, ocean circulation is organized into large gyres, just like in the modern oceans, including the North Pacific, South Pacific, North Atlantic, South Atlantic and Indian gyres (Figure 2D). The location, orientation and intensity of the gyres are identical for all three simulations. However, the circumpolar current is slightly less intense in the Mio300Dust simulation, with a mean flow of 79 Sv, compared to 92 and 90 Sv for the Mio420Dust and Mio560Dust simulations (not shown).

3 Results

3.1 Geographical distribution of productivity anomalies

3.1.1 Description of global primary productivity distribution

The spatial distribution of annual primary productivity is similar in all simulations (Figure S1). In the eastern Pacific Ocean, the high productivity is mainly located in the equatorial zone, exceeding 1 g/m²/day in some areas (Figure 3A and 2B). This area, surrounded by two oligotrophic zones, corresponds to an important site of upwelling activity. Other productive areas are located in the western part of the basin, off the coasts of Southeast Asia and Australia. The coasts of the Indian Ocean are rich in productivity, raising the level of the entire basin, with the exception of an oligotrophic belt extending along 15°S of latitude between Madagascar and Australia (less than 0.1 g/m²/day). In the Atlantic Ocean, waters close to the African coast have a high rate of productivity, just like waters close to Central America. Other productive areas are located in a zone between North America and Europe (at around 40°N) and between South America and Africa (at around 40°S). The Arctic and Southern Oceans exhibit low primary productivity in the simulations. In all simulations, this productivity comes mainly from nanophytoplankton, except in a few areas such as the polar oceans or some parts of the Pacific Ocean, where diatoms predominate (Figure S2, S3, S4).

3.1.2 Global distribution of dust-induced anomalies

Adding dust to the model significantly increase primary productivity in the simulations. In the Mio420NoDust simulation, the overall mean primary productivity is 0.32 g/m²/day, compared to 0.35 g/m²/day in the Mio420Dust simulation (Table 1). The main anomalies are located in the Atlantic and Indian Oceans, and more specifically in the waters off the coast of Africa (Figure 3C). Two areas exceed +0.2 g/m²/day and are located off the coast of North Africa (between the Gibraltar strait and Cape Verde archipelago) and in the Arabian Sea. This is due to the spatial distribution of dust, which is highly concentrated near Africa, at the vicinity of Sahara desert. The increase in productivity in the Pacific Ocean is more heterogeneous than in other basins. In this zone, dust-derived nutrients arrive mainly via ocean currents (from other oceanic basins). The primary productivity generated by equatorial upwelling in the eastern part of the basin decreases with the increase in dust input. This behavior is also simulated along coastlines in the western and eastern part of the basins (i.e. north-western coast of North America, north-eastern coast of South America, Australian coasts, Mediterranean Sea).

3.1.3 Global distribution of pCO₂-induced anomalies

Temperature decrease triggers a global decrease in primary productivity, from 0.38 g/m²/day on average for the Mio560Dust simulation to 0.33 g/m²/day on average for the Mio300Dust simulation (Table 1). The signal is strongest in the Atlantic Ocean, with anomalies exceeding -0.2 g/m²/day in some places (i.e. Gulf of Mexico, Figure 3 D). Productivity in the Indian Ocean is also declining, especially around 15°S. While there is also a significant anomaly in the north-western Pacific Ocean, other parts of the basin show a less clear signal. In the eastern Pacific Ocean, productivity increases with decreasing temperature in some

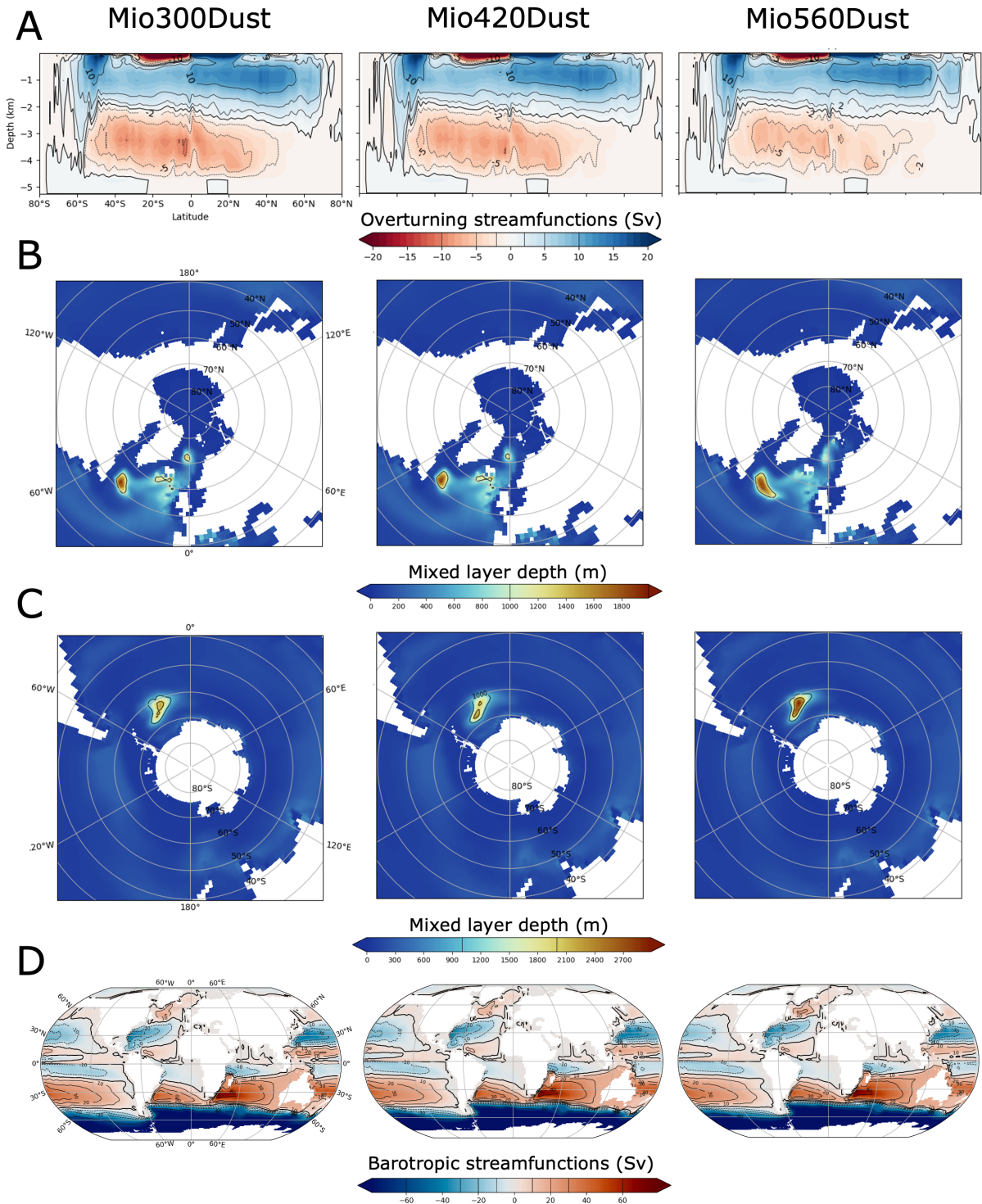


Figure 2. Left column, Mio300Dust simulation. Middle column, Mio420Dust simulation. Right column, Mio560Dust simulation. (A) Global Meridional Overturning Circulation (MOC), in Sverdup (Sv, $1 \text{ Sv} = 10^6 \text{ m}^3/\text{s}$), computed from the global ocean. (B) Mixed layer depth (mld, meter) averaged over the winter (January-February-March). (C) Mixed layer depth (meter) averaged over the austral winter (July-August-September). (D) Mean annual barotropic stream function (Sv). In red, the water masses rotate counterclockwise and in blue, clockwise. Values represent average on the last 100 years of each simulation.

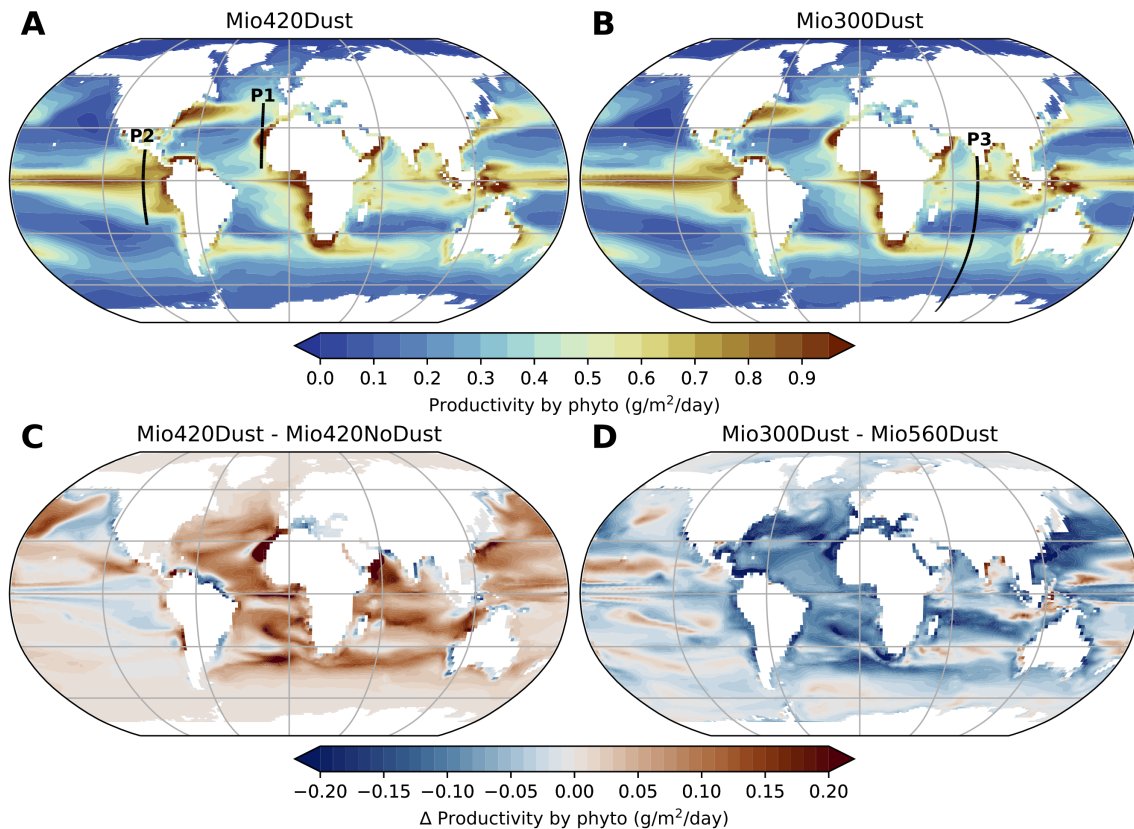


Figure 3. Ocean primary productivity by phytoplankton integrated through the water column and averaged over the year ($\text{g/m}^2/\text{day}$). A: Mio420Dust simulation. B: Mio300Dust simulation. C: Difference between Mio420Dust and Mio420NoDust simulations. D: Difference between Mio300Dust and Mio560Dust simulations.

248 areas. The spatial distribution of these zones is highly heterogeneous, with a significant
 249 positive anomaly between $0\text{-}30^\circ\text{N}$ and $160^\circ\text{E}\text{-}120^\circ\text{W}$. The coastal signal, on the other hand,
 250 is globally negative, with a decrease in productivity between Mio560Dust and Mio300Dust.

251 **3.2 Direct impact of dust : the example of North-western African coastlines** 252 **(Atlantic Ocean)**

253 In order to emphasize mechanisms at play we decide to focus our analysis on regional
 254 scale. As mentioned previously, the area where the anomaly is most pronounced for the dust
 255 sensitivity experiments is located in the sub-tropical Atlantic Ocean, off the north-western
 256 African coast (around 20°W and $15\text{-}30^\circ\text{N}$, Figure 4A,B). In this area, productivity is mainly
 257 limited to the first 100 meters of the water column (below this depth, light is a limiting
 258 factor), and its vertical profile follows isodensity lines (Figure 4A) and local currentology
 259 (Figure 4D). Productivity in this zone comes mainly from nanophytoplankton (Figure 4C),
 260 whose biomass dominates that of diatoms. In this area, adding dust to the simulation (i.e.
 261 transition from Mio420NoDust to Mio420Dust) does not change the overall spatial distri-
 262 bution of productivity, but does increase productivity in already productive areas. The
 263 maximum increase is found between 0 and 50m depth and between 20 and 25°N , reaching
 264 $+0.5 \text{ g/m}^3/\text{day}$ with the addition of dust. The vertical profile of nutrient limitation (Fig-

265 ure 4E) shows that nutrients are much less limiting at this location than further north or
 266 south. The difference in nutrient limitation between the two simulations shows that at this
 267 location, nutrients are less of a limiting factor in the Mio420Dust simulation than in the
 268 Mio420NoDust simulation (Figure 4F). This very localized increase is therefore certainly
 269 due to the influx of dust from North Africa (Sahara desert) bringing nutrients to the surface
 270 ocean (Figure 1B). This correlation between productivity and dust is both geographical
 271 (as shown above) and temporal. Annual time series in this zone show that primary pro-
 272 ductivity trends are seasonal (Figure 5A). It increases in autumn, peaks in winter, then
 273 decreases during spring to reach its minimum at the end of summer. This annual cycle is
 274 flattened with decreasing dust: seasonal amplitude is more pronounced in the Mio420Dust and
 275 Mio420Dust2 simulations than in the Mio420Dust10 and Mio420NoDust simulations. This
 276 evolution of primary productivity follows very closely the evolution of the nutrient limitation
 277 term (Figure 5B). The concentration of dust in the atmosphere and its deposition in the
 278 oceans also varies according to the month of the year (Figure 5C). In the concerned area,
 279 nutrient deposition via dust increases strongly in winter/early spring and decreases in sum-
 280 mer. Primary productivity follows the same seasonal cycle as dust deposition, highlighting
 281 a geographical and temporal correlation between the two parameters.

282 **3.3 Remote effect of dust supply : the example of the Eastern Equatorial** 283 **Pacific**

284 Some areas, such as the EEP, show a decrease in primary productivity in response to
 285 an increase in dust supply. EEP shows a decrease in productivity between 10°N and 20°S
 286 between our Mio420NoDust and Mio420Dust simulations, with the exception of a thin band
 287 around the equator. The profile on Figure 6A shows that primary productivity in the EEP
 288 remains localized above 100m depth. At the surface, primary productivity comes mainly
 289 from nanophytoplankton, but the proportion of diatoms increases with depth in the water
 290 column (Figure 6C). The productivity anomaly between Mio420Dust and Mio420NoDust
 291 shows that positive anomaly zones (i.e., an increase in productivity following an increase
 292 in dust) are located around 25°S, 0° and 15°N (Figure 6B). Negative anomalies are located
 293 between 0° and 20°S and between 0° and 10°N, and remain below the 1024 kg/m³ isodensity
 294 line. This pattern of positive and negative productivity anomalies follows the nutrient
 295 limitation anomalies and location of major downwelling and upwelling (Figure 6F). In this
 296 region, the downwelling cells are indeed localized respectively at 25°S and at 15°N while a
 297 main upwelling brings the waters upwards near the equator (Figure 6D). As seen previously,
 298 nutrients enter this basin mainly via oceanic circulation, rather than via direct input from
 299 dust by atmospheric circulation. A primary productivity increase that would use available
 300 nutrients at one place, would subsequently lead to a decrease in nutrients supply to other
 301 regions. This is what happens in the EEP: additional nutrient supply, due to global increase
 302 in dust input to the ocean, lead to increase productivity in downwelling and upwelling
 303 zones (25°S, 0° and 15°N), which result in water transported to adjacent region via lateral
 304 Ekman transport to be nutrient-depleted, reducing nutrient content of those waters (between
 305 0° and 20°S and between 0° and 10°N). This is why, in the Mio420NoDust simulation,
 306 the latitudinal distribution is more homogeneous, as there are less zones of productivity
 307 (consuming nutrients) and therefore more nutrients between these zones.

308 **3.4 Impact of temperature: Focus on the Indian Ocean**

309 In order to highlight the mechanisms linking temperature and productivity, we decided
 310 to focus on the Indian Ocean, where the spatial distribution of the anomaly for the pCO₂
 311 sensitivity experiments is particularly heterogeneous (Figure 3D). In this oceanic basin, de-
 312 creasing atmospheric pCO₂ mostly leads to a drop in primary productivity. We decide, for
 313 further analysis, to focus on a profile along 77° E, along which the productivity response
 314 varies. In the Mio300Dust simulation, between India and Antarctica, the vertical profile
 315 of productivity shows two areas of high production: one south of India (between 10°N and

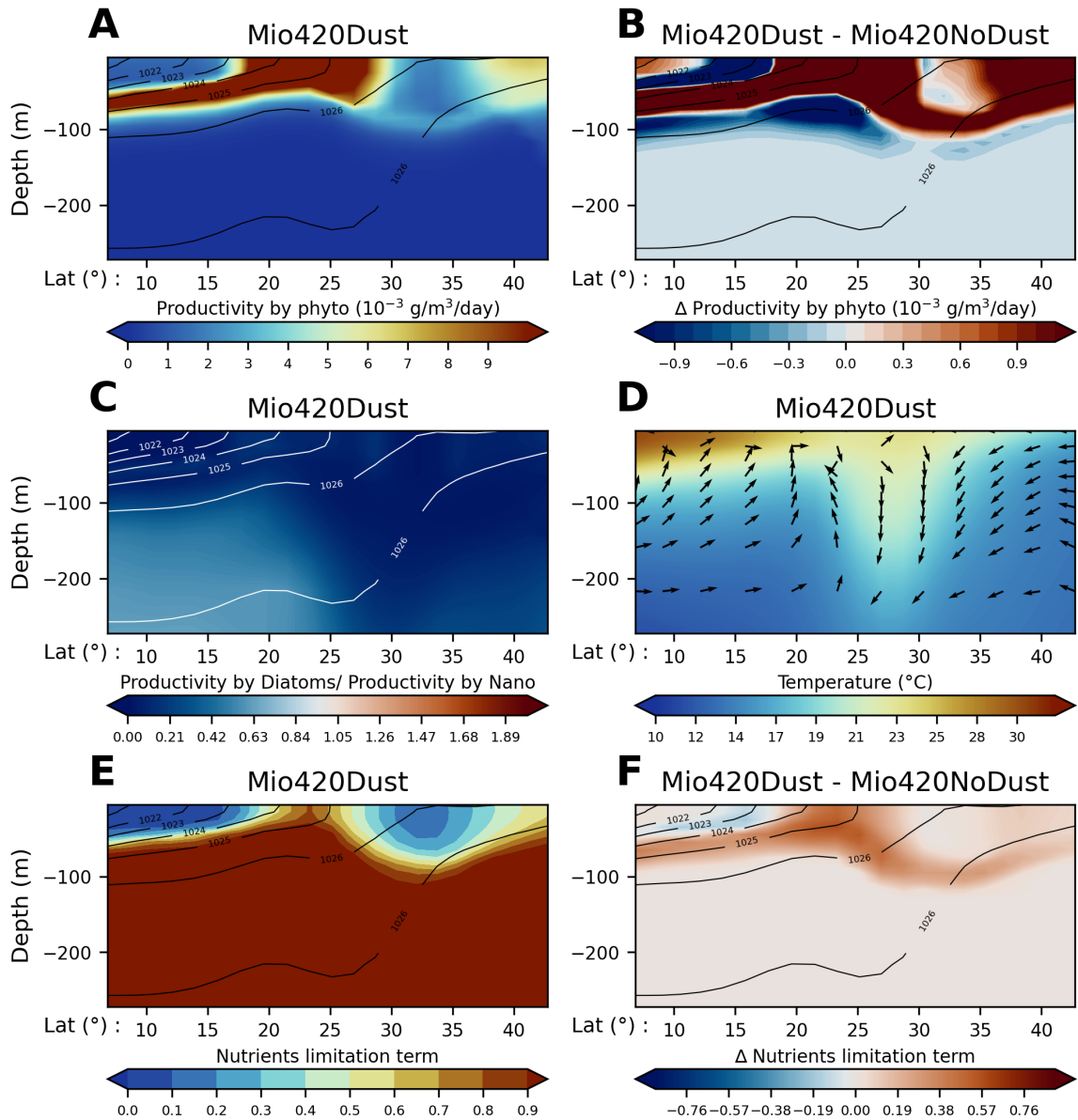


Figure 4. P1 profile, along north-western African coastlines (17°W and 5-42°N, Figure 3A), as a function of latitude (horizontal axis) and depth in meters (vertical axis). A: Phytoplankton Primary productivity averaged over the year ($\text{g/m}^2/\text{day}$) with isodensity lines in black (kg/m^3) for the Mio420Dust simulation. B: Difference in phytoplankton primary productivity averaged over the year ($\text{g/m}^2/\text{day}$) between the Mio420Dust and Mio420NoDust simulations (with isodensity lines in black in kg/m^3 for Mio420Dust). C: Ratio between primary productivity produced by diatoms and primary productivity produced by nanophytoplankton for the Mio420Dust simulation (if >1 , diatom dominance, if <1 , nanophytoplankton dominance) with isodensity lines in white in kg/m^3 (for Mio420Dust). D: Water temperature ($^{\circ}\text{C}$) with arrows representing normalized Eulerian mass transport for the Mio420Dust simulation. E: Nutrient limitation term for nanophytoplankton (between 0 and 1) for the Mio420Dust simulation. The closer the term is to 0, the more nutrients limit nanophytoplankton development (with black isodensity lines in kg/m^3 for Mio420Dust). F: Differences in nutrient-limiting term for nanophytoplankton between the Mio420Dust simulation and the Mio420NoDust simulation (with black isodensity lines in kg/m^3 for Mio420Dust).

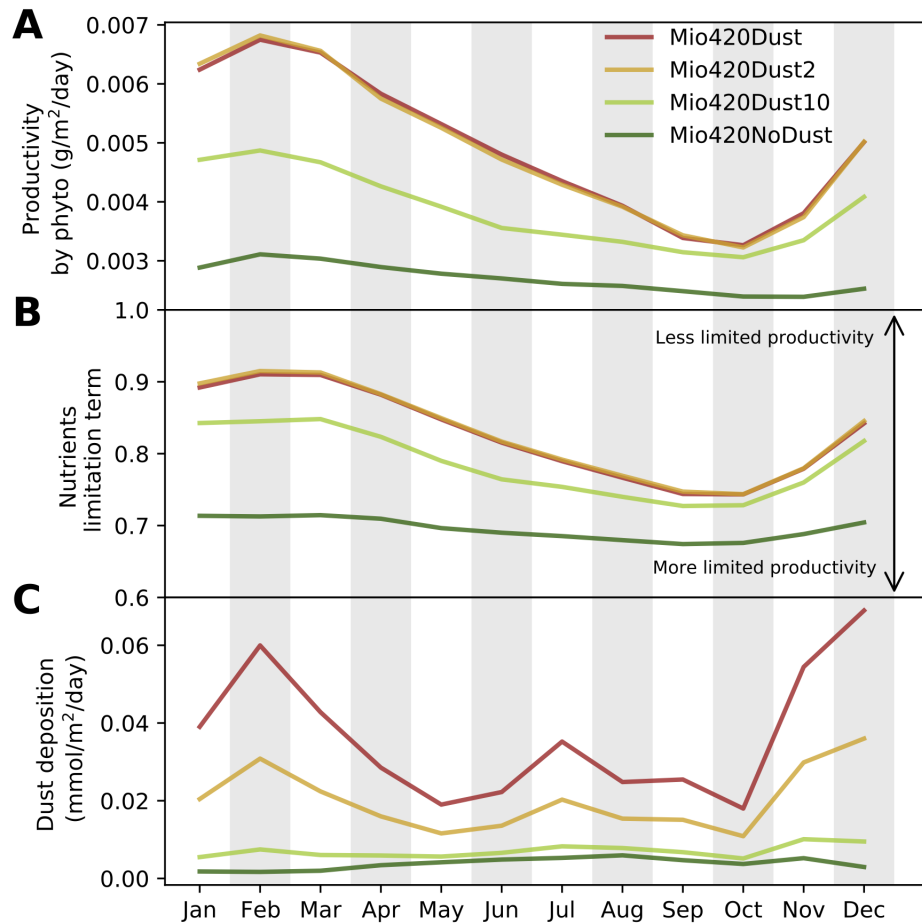


Figure 5. Annual variation of (A) Primary productivity by phytoplankton ($\text{g}/\text{m}^2/\text{day}$) ; (B) Nutrient limitation term (The closer the term is to 0, the more nutrients limit nanophytoplankton development) and (C) Dust deposition (Silica + Nitrogen + Phosphorus + Iron) ($\text{mmol}/\text{m}^2/\text{day}$) for Mio420Dust, Mio420Dust2, Mio420Dust10 and Mio420NoDust simulations. Values are averaged over an area corresponding to profile P1, along north-western African coastlines (17°W and $5\text{--}42^\circ\text{N}$, Figure 3A).

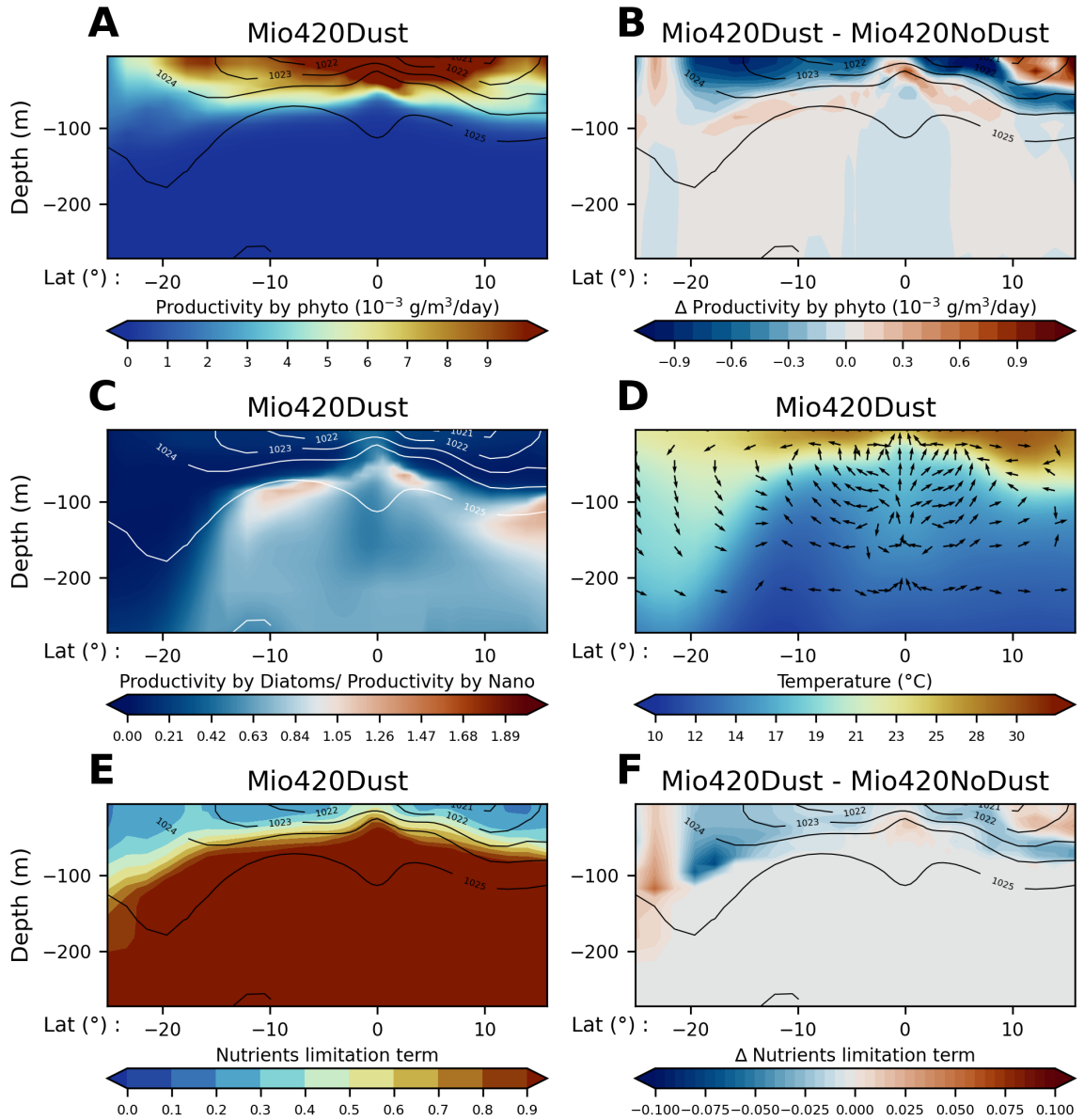


Figure 6. P2 profile, in the EEP (93°W and 25°S-15°N Figure 3A), as a function of latitude (x-axis) and depth in meters (y-axis). A: Primary phytoplankton productivity averaged over the year ($\text{g}/\text{m}^2/\text{day}$) with isodensity lines in black (kg/m^3) for the Mio420Dust simulation. B: Difference in phytoplankton primary productivity averaged over the year ($\text{g}/\text{m}^2/\text{day}$) between the Mio420Dust and Mio420NoDust simulations (with isodensity lines in black in kg/m^3 for Mio420Dust). C: Ratio between primary productivity produced by diatoms and primary productivity produced by nanophytoplankton for the Mio420Dust simulation (if >1 , diatom dominance, if <1 , nanophytoplankton dominance) with isodensity lines in white in kg/m^3 (for Mio420Dust). D: Water temperature ($^{\circ}\text{C}$) for the Mio420Dust simulation with arrows representing normalized Eulerian mass transport for the Mio420Dust simulation. E: Nutrient limitation term for nanophytoplankton (between 0 and 1) for the Mio420Dust simulation. The closer the term is to 0, the more nutrients limit nanophytoplankton development (with black isodensity lines in kg/m^3 for Mio420Dust). F: Differences in nutrient-limiting term for nanophytoplankton between the Mio420Dust simulation and the Mio420NoDust simulation (with black isodensity lines in kg/m^3 for Mio420Dust).

316 10°S) with a maximum depth of 100m, and another further south (at around 40°S) with a
 317 maximum depth of 200m (Figure 7A). These two areas are split by a low productivity area
 318 (between 20° and 30°S) corresponding to the oligotrophic gyre of the South Indian Ocean
 319 (Figure 3B and Figure 7C). There is, however, a productivity belt at around 120m depth,
 320 following the isodensity lines. The vertical profile of productivity difference between the
 321 Mio300Dust and Mio560Dust simulations shows a very heterogeneous signal (Figure 7B),
 322 but with a majority of areas where productivity decreases as temperature decreases. Sur-
 323 face temperatures are on average -2.5°C colder in Mio300Dust (Figure 1C) and this anomaly
 324 extend deeper (Figure 7D). Ammonium (NH_4^+) is a nitrogen form released during reminer-
 325 alization and used as nutrient for primary productivity. The vertical profile of ammonium
 326 concentration follows a distribution similar to productivity in the Mio300Dust simulation
 327 (Figure 7E) and there is a decrease in ammonium concentration in the Mio300Dust com-
 328 pared to the Mio560Dust simulation (Figure 7F). This decrease in ammonium concentration
 329 is caused by a decrease in remineralization, which follows the temperature drop (Figure 7D).
 330 Over the whole simulation, at global scale, productivity decreases on average by 13% be-
 331 tween Mio560Dust and Mio300Dust (Table 1), while carbon export at 100m depth only
 332 decreases by 7%. This difference in anomaly is due to remineralization, which recycles part
 333 of the productivity before it is exported downwards.

334 4 Discussion

335 4.1 Comparison of results with other modelling studies

336 Previous studies using marine biogeochemistry modelling have investigated the impact
 337 of dust on primary productivity in the context of future climatic projections (Dutkiewicz
 338 et al., 2005; Tagliabue et al., 2008, 2009) or for the Last Glacial Maximum (Bopp et al.,
 339 2003; Lambert et al., 2015). Tagliabue et al. (2008) also used the PISCES model to run
 340 transient simulations focusing on the impact of dust input reduction on future oceans. In
 341 their simulations, a 60% reduction in dust input leads to a 3% drop in primary productivity
 342 in the oceans. In our case, a 50% decrease in dust (from Mio420Dust to Mio420Dust2, Table
 343 1) results in a 2.9% decrease in primary productivity, which is consistent with their results.
 344 However, the geographical distribution of productivity anomalies is different between the
 345 two studies (as in the Southern Ocean), certainly due to the difference in ocean circulation
 346 patterns between the Miocene and the present-day. Dutkiewicz et al. (2005) simulated a
 347 decrease in productivity of less than 10% in response to a 10-fold drop in dust levels, using an
 348 ocean circulation model coupled with a biogeochemical model. In comparison, productivity
 349 fell by 6% between the Mio420Dust and Mio420Dust10 simulations (Table 1). The negative
 350 correlation we simulate for the EEP in the Mio420Dust and Mio420NoDust simulation is
 351 featured as well in previous study from the literature but in the Atlantic basin. This negative
 352 correlation can be explained by oceanic circulation and has already been mentioned by Bopp
 353 et al. (2003) and Tagliabue et al. (2008). The phenomenon of increased primary productivity
 354 using the nutrients available in one place, resulting in a reduced supply of nutrients in other
 355 areas, was mentioned in Aumont et al. (2003). This same process may explain the negative
 356 coastal productivity anomalies between Mio420Dust and Mio420NoDust simulation at the
 357 continental margins of Asia and South America (for example through coastal upwelling
 358 systems).

359 Previous studies also look at the effect of pCO_2 change on primary productivity focus-
 360 ing mainly on future climate warming and its impact on primary productivity. In a model
 361 intercomparison study, (Steinacher et al., 2010) highlight a global decline in primary pro-
 362 ductivity (varying between 2% and 20% depending on the model) by 2100 in response to
 363 anthropogenic global warming. Authors attribute this decrease to warming-induced changes
 364 in ocean circulation: a slower ocean circulation, a reduced depth of the mixing layer and an
 365 increased stratification lead in the simulations to a decrease in the supply of nutrients to
 366 surface waters (with the exception of the Southern Ocean). A similar overall decrease in pro-
 367 ductivity in response to increasing temperature are found in other modeling studies (Cabr e

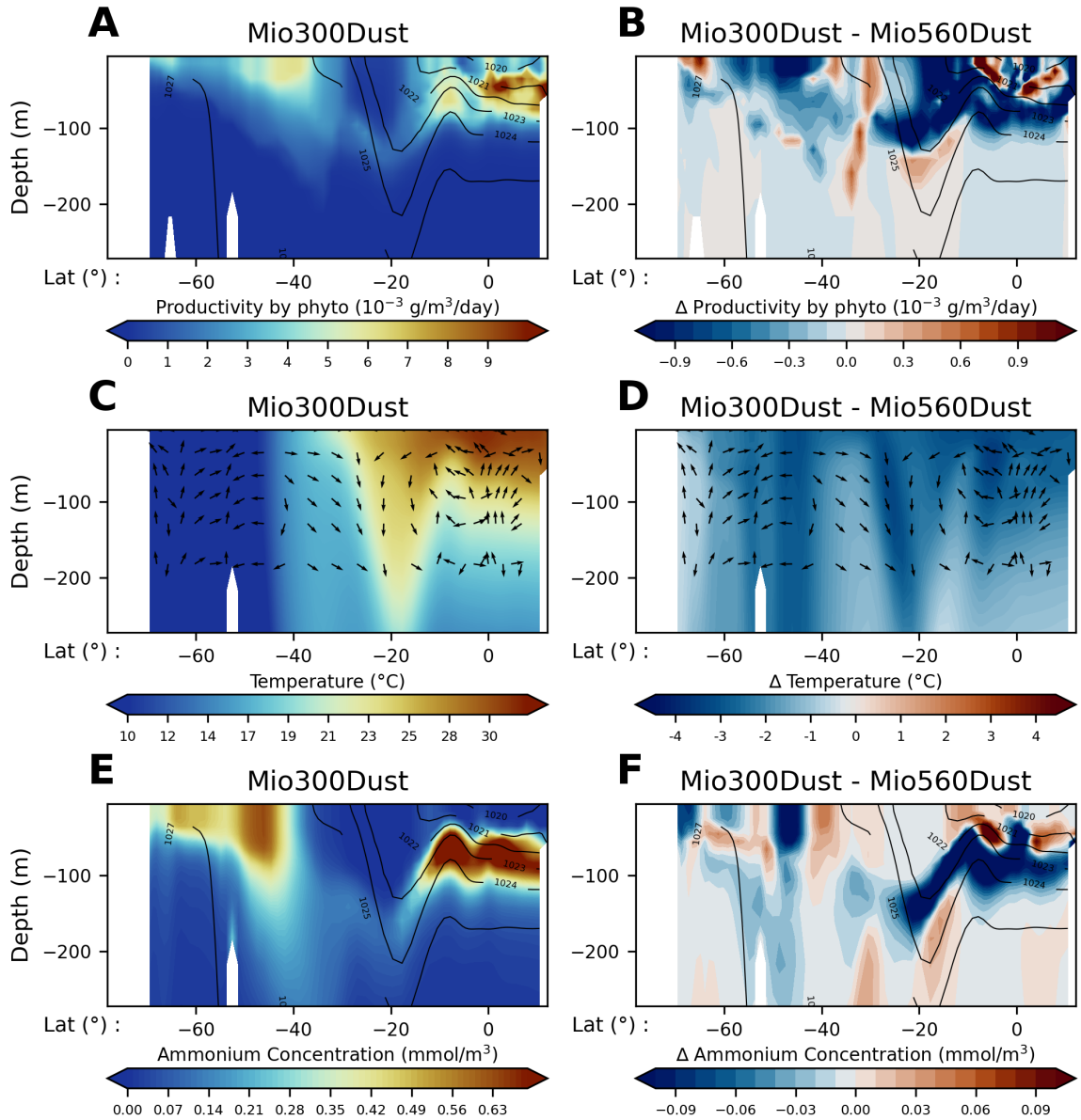


Figure 7. P3 profile, between India and Antarctica (77°E and 80°S-10°N, Figure 3B) as a function of latitude (x-axis) and depth in meters (y-axis). A: Phytoplankton primary productivity averaged over the year ($\text{g/m}^2/\text{day}$) with isodensity lines in black (kg/m^3) for the Mio300Dust simulation. B: Difference in phytoplankton primary productivity averaged over the year ($\text{g/m}^2/\text{day}$) between the Mio300Dust and Mio560Dust simulations (with isodensity lines in black in kg/m^3 for Mio300Dust). C: Water temperature ($^{\circ}\text{C}$) for the Mio300Dust simulation with arrows representing normalized Eulerian mass transport for the Mio300Dust simulation. D: Difference in water temperature ($^{\circ}\text{C}$) between the Mio300Dust and Mio560Dust simulations (with arrows representing normalized Eulerian mass transport for the Mio300Dust simulation). E: Ammonium concentration (mmol/m^3) for the Mio300Dust simulation (with isodensity lines in black in kg/m^3 for Mio300Dust). F: Difference in ammonium concentration (mmol/m^3) between Mio300Dust and Mio560Dust simulations (with black isodensity lines in kg/m^3 for Mio300Dust).

368 et al., 2015; Sarmiento et al., 2004; Kwiatkowski et al., 2019). Laufkötter et al. (2015)
 369 analyzed the changes in primary productivity simulated by nine models in the context of
 370 anthropogenic warming to 2100 (RCP8.5, IPCC). Most of the models present (including two
 371 versions of PISCES model from Aumont and Bopp (2006)) simulate a decrease in primary
 372 productivity. They find that the decrease in productivity simulated with PISCES model is
 373 mainly due to a decrease in nutrient supply following an increase in water stratification. For
 374 the other models, the simulated decrease in productivity is rather due to a warming-induced
 375 increase in grazing pressure. From Laufkötter et al. (2015), one model (PlankTOM5.3 from
 376 Buitenhuis et al. (2013)) simulates an increase in primary productivity in response to in-
 377 creasing temperature. The productivity changes simulated with PlankTOM5.3 are very
 378 different from changes in export production. The authors attribute this to a very strong
 379 increase in recycling efficiency (remineralization) in this model in response to a temperature
 380 increase. The importance of temperature effect on remineralization have been highlighted
 381 in Crichton et al. (2021) who used the cGENIE.muffin model with a temperature-dependent
 382 representation of the marine carbon cycle. In our simulation (Mio300Dust vs Mio560Dust),
 383 productivity rather decreases with decreasing temperature. We observe no clear differ-
 384 ence in stratification between Mio300Dust and Mio560Dust simulations (Figure S6), this is
 385 because our simulations have been running for 3,000 years and have therefore reached an
 386 equilibrium state, even in the deep ocean. This homogenization of the temperature anomaly
 387 over the whole water column is not necessarily present in transient simulations lasting only
 388 100 years and with a time varying forcing, as is the case in Laufkötter et al. (2015) or in
 389 (Steinacher et al., 2010). In our simulations, temperature has a major effect through rem-
 390 ineralization (Figure 7), although we cannot totally exclude that a slight change in ocean
 391 dynamics forced by a decrease water temperature has an impact on primary productivity.
 392 Difference between our results and those published modeling work may stem from multiple
 393 factors: 1) The initial conditions of the sensitivity test (background state is different due to
 394 different initial $p\text{CO}_2$ and geography). 2) The model used and its productivity scheme, as
 395 seen previously (Steinacher et al., 2010; Laufkötter et al., 2015) and the simulation length
 396 (100 years vs. 3000 years). 3) Miocene ocean circulation that is different from the present-
 397 day one (Steinthorsdottir et al., 2021), affecting nutrient distribution. Primary productivity
 398 in PISCES is highly sensitive to changes in ocean circulation induced by the opening of a
 399 seaway (Ladant et al., 2018).

400 4.2 Carbon export and the Late Miocene Biogenic Bloom

401 As we show previously, primary productivity rarely extend below 100m depth (Figure
 402 4A, Figure 6A, Figure 7A). Particulate carbon export at 100m depth increases by an average
 403 of 12.5% in response to dust deposition (Table 1). Spatial distribution of annual particulate
 404 carbon export at 100m is similar in all simulations (Figure S5). The spatial distribution of
 405 the carbon export anomaly between Mio420NoDust and Mio420Dust (Figure 8A) matches
 406 that of primary productivity (Figure 3C) and shows a heterogeneous spatial distribution.
 407 The difference is the most pronounced in the Atlantic Ocean, reaching $+0.1 \text{ g/m}^2/\text{day}$ off
 408 the North African coast. Areas that show a decrease in productivity in response to dust
 409 addition (e.g. EEP) also show a slight decrease in carbon export. We suggest that the
 410 increase in carbon export we simulate could correspond to an event like the LMBB, as this
 411 is characterized, among other aspects, by an increase in calcite accumulation in sediments.
 412 The spatial distribution of sites where this event has been observed (Pillot et al., 2023)
 413 also shows considerable heterogeneity, with sites labelled "LMBB" (in red on Figure 8)
 414 sometimes very close to sites labelled "no LMBB" (in blue on Figure 8). Geographical
 415 superimposition shows that sites labelled "LMBB" can be found in areas where simulated
 416 carbon export is increasing (e.g. South Atlantic Ocean, Australian coasts, Indian Ocean,
 417 North Pacific), but also in areas where carbon export is decreasing (EEP, South American
 418 coasts). On the other side, sites with no evidence for LMBB ("no LMBB" label) are also
 419 sometimes located in areas where simulated carbon export is changing significantly (i.e.
 420 Atlantic Ocean). The simulations show very small changes in carbon export in the Southern

Ocean, which is in agreement with the compilation of data showing no evidence of LMBB in this part of the ocean. The spatial heterogeneity of the compilation makes site-by-site model-data correlation difficult, however the scenario of increased dust supply to explain the onset of LMBB is supported by the fact that 1) most of the sites where the LMBB was identified are located in areas of simulated carbon export increase (Figure 8B) and 2) the spatial distribution of the carbon export anomaly is heterogeneous, and this is also the case for the compilation. This result tend to support Diester-Haass et al. (2006) which show a correlation between the evolution of paleoproductivity in the Late Miocene-early Pliocene in the EEP (site ODP 846, near the equator) and the evolution of wind-driven dust in this area (site ODP 848, calculated by Hovan (1995)). Crocker et al. (2022) observed an increase in dust flux in North Atlantic sediments (ODP site 659) from 8 to 5 Ma, coinciding with the onset of the LMBB between 8 and 6.5 Ma. In the Miocene, dust might also come from an external origin, such as the break-up of an asteroid, which caused an interplanetary dust particles shower on the Earth's surface around 8 Ma (Farley et al., 2006), coinciding temporally with the onset of the LMBB. However, further flux calculation are needed to evaluate the reliability of extraterrestrial supply as oceanic fertilizer. In this scenario, the distribution of dust deposits would be more homogeneous in the oceans and not linked to present-day deserts, as is the case in our study.

Our sensitivity tests for change in ppCO_2 show a global mean decrease of 7% in carbon export at 100m for a pCO_2 decrease of 260ppm and a global mean SST decrease of 2.5°C (Table 1). The spatial distribution of anomalies is more heterogeneous than in the dust sensitivity test (Figure 8C), but follows also the primary productivity anomaly patterns (Figure 3D). The main areas of decreasing carbon export are located in the Atlantic Ocean, the Indian Ocean (between 10° and 30°S) and the north-western Pacific Ocean. There are also areas where carbon export increases in response to lower pCO_2 , such as in the EEP, the northern Indian Ocean and around Southeast Asia. The decline in Biogenic Bloom corresponds, among other things, to a decrease in calcite accumulation in marine sediments. This could be linked, in part, to the cooling associated with global drop in the partial pressure of ppCO_2 in the atmosphere during the Late Miocene. This hypothesis is supported by the carbon export calculated for each "LMBB" site, which is on average lower in the Mio300Dust simulation than in Mio560Dust (Figure 8D). As in the dust supply sensitivity experiments, the heterogeneity of the signal makes the geographical correlation between modeled carbon export and LMBB distribution according to Pillot et al. (2023) complex. Sites with recorded LMBB are found where simulated carbon export decreases (e.g. Atlantic Ocean) but also increases (e.g. EEP), in response to a decrease in pCO_2 . Superimposing the two effects (dust supply increase + pCO_2 decrease) shows an even more heterogeneous spatial distribution of carbon export (Figure 8E). The carbon export anomaly between Mio420NoDust and Mio300Dust shows more areas corresponding to an increase in carbon export (e.g. Atlantic Ocean, Indian Ocean, EEP, North Pacific Ocean). However, the average carbon export calculated at sites labelled "LMBB" is very close to zero (Figure 8F), showing a compensatory effect of the two sensitivity tests. In summary, we could use this simulations to propose a three-stage scenario to explain the temporal evolution of the LMBB: 1) The onset of the LMBB between 8 and 6.5 Ma explained by the increase in dust deposits in the ocean linked to global aridification. During this period, the role of dust predominated over the role of pCO_2 . 2) The event's maximum at around 6.5 Ma marks a balance between the effects of dust and pCO_2 . 3) The decline of the LMBB between 6.5 and 2 Ma, explained by the decrease in ocean temperature (except for a short temperature increase in high latitudes around 5Ma, Herbert et al. 2016), linked to a drop in pCO_2 levels. During this period, the role of pCO_2 could have predominated over the role of dust. However, it is important to note that there are limited constraints on the temporal evolution of these two forcings, making it difficult to determine the reasons for one dominating the other. Some possible improvements to the scenario are discussed in the next subsection.

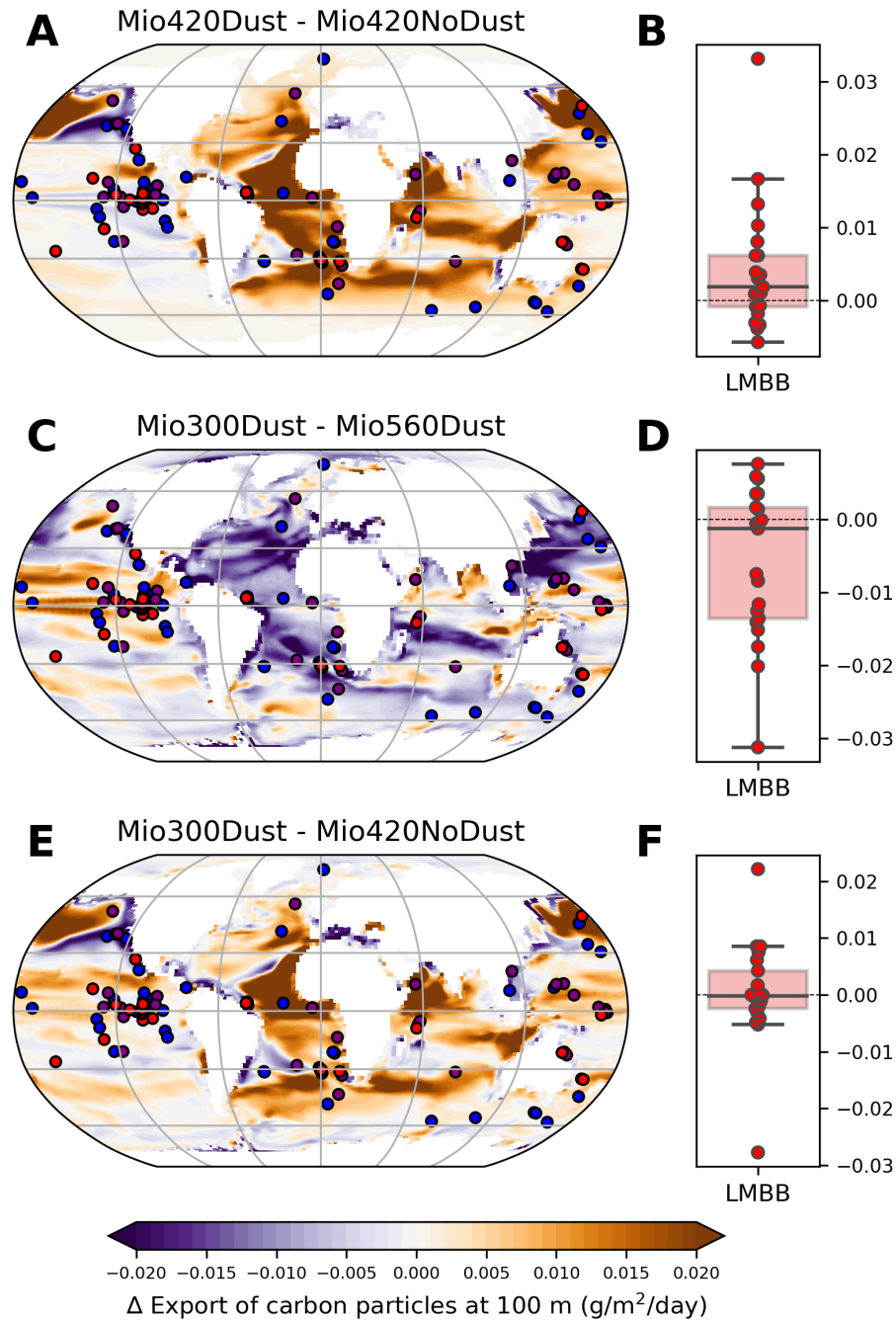


Figure 8. A), C) and E) Differences in particulate carbon export at 100m depth ($\text{g}/\text{m}^2/\text{day}$) and averaged over the year. Blue - no LMBB; purple - controversial LMBB; red - LMBB present. Dots show paleo-positions at 10 Ma of labeled sites reporting the presence or absence of LMBB, from the compilation of Pillot et al. (2023). B), D) and F) box plot showing for each site labelled "LMBB" the simulated particulate carbon export anomaly at 100m depth ($\text{g}/\text{m}^2/\text{day}$) calculated at the site paleo-location (10 Ma). A) and B) Mio420Dust - Mio420NoDust. C) and D) Mio300Dust - Mio560Dust. E) and F) Mio300Dust - Mio420NoDust.

4.3 Limitations and perspectives

Although the scenario proposed above is temporally consistent with some studies, it does not take into account several continental and oceanic parameters that evolved significantly during the Late Miocene and Pliocene, some of which have been attributed as potential causes of the LMBB. First, ocean circulation, which changed significantly during this time period, notably due to paleogeographic changes (Herold et al., 2012). Oceanic circulation in the Late Miocene and Pliocene is partly driven by North Atlantic Deep Water (NADW) formation, whose dynamics has been shown to be influenced by many geographic component that evolved during the Late Miocene to Pliocene. This make individual contributions difficult to quantify (Poore et al., 2006) and no continuous record of NADW strength exist over the entire interval. The NADW might have underwent phases of decreasing intensity, as modeled by Brierley and Fedorov (2016) in response to the sudden opening of the Bering Seaway in the early Pliocene (Gladenkov & Gladenkov, 2004; Hall et al., 2023). Phases of uplift and subsidence of the Greenland-Scotland Ridge in the Late Miocene likely caused periodic variations in NADW production (Hossain et al., 2020; Poore et al., 2006; Wright & Miller, 1996). The NADW might have been intensified by the closure of the Central American seaway (Nisancioglu et al., 2003; Schneider & Schmittner, 2006; Sepulchre et al., 2014), whose exact timing though remains debated (Molnar, 2008, 2017; Montes et al., 2015; O’Dea et al., 2016), but also by the progressive development of an ice sheet over Greenland (Pillot et al., 2022; Davini et al., 2015) for which evidences exist since 7.5 Ma (Bierman et al., 2016). In addition to NADW, phases of onset and collapse of deep-water formation in the North Pacific (NPDW) also occurred during the late Miocene and Pliocene, varying the proportion of deep water from the North Atlantic and North Pacific Oceans in the meridional overturning circulation (Abell & Winckler, 2023; Ford et al., 2022; Burls et al., 2017). Those factors impacting circulation are not all taken into account in our study as it would require additional sensitivity experiments for each to them; but they could have a drastic impact of the geographic distribution of nutrients or the intensity of upwelling, both impacting primary productivity. We though suspect that although patterns of increased/decreased productivity could be different in some other simulations, the mechanisms we evidenced should still be valid (decrease nutrient limitation with increasing dust input and decrease remineralization with decreasing temperature).

In addition to the circulation changes mentioned above and the increase in dust deposition (as investigated in this study), the evolution of nutrient supply by rivers may have also impacted primary productivity at this time. In our study we have kept the quantity of nutrients transported by rivers from the continents to the ocean constant among simulations, regardless of the dust quantity in the atmosphere or the atmospheric pCO₂. The latter should affect the intensity of the runoff due to change in temperature that affect the capacity of atmosphere to hold water and therefore the hydrological cycle (Herold et al., 2011). Previous studies show evidences for change in river input of nutrient throughout the Late Miocene and Pliocene. First, some studies suggest an increase in continental weathering associated to late uplift in the Tibetan Plateau (Wang et al., 2014; Clift et al., 2020; Filippelli, 1997; Holbourn et al., 2018; Yang et al., 2019) and the uplift of the Andes at 8 Ma (Hermoyian & Owen, 2001; Curry, WB and Shackleton, NJ and Richter, C and Backman, JE and Bassinot, F and Bickert, T and Chaisson, WP and Cullen, JL and deMenocal, P and Dobson, DM and others, 1995). Secondly, river nutrient supply might have been affected by the increased input of siliceous phytoliths into the ocean due to the global spread of C4 plants (Pound et al., 2012). Moreover, the LMBB is also characterized by an increase in the export of biogenic silica (opal) in several sites of the Pacific Ocean (Cortese et al., 2004). Thirdly, in our simulation we kept orbital parameters in present day configuration but this parameter (which has a higher temporal resolution than the factors mentioned previously) can affect the intensity of the hydrological cycle (Tardif et al., 2021). A particular orbital configuration can lead to a change in insolation intensity impacting continental weathering (Karatsolis et al., 2022). Orbital parameters can also have a direct impact on dust deposition (Crocker et al., 2022) and the distribution of primary productivity (Le Mézo et al., 2017;

527 Beaufort et al., 2022). The evolution of nutrient supply by rivers may have contributed sig-
 528 nificantly to the evolution of global primary productivity in the Late Miocene and Pliocene.
 529 In order to clearly identify the roles of all these parameters on the onset and ending of the
 530 LMBB, further studies should focus on the impact of different mode of ocean circulation
 531 and change in runoff on primary productivity in the Late Miocene-Pliocene oceans. We
 532 also need more data with land-ocean continuum records of productivity, dust and detrital
 533 material covering the late Miocene and Pliocene.

534 5 Conclusion

535 Our simulations suggest that the evolution of marine primary productivity at the end of
 536 the Miocene could have been impacted by aridification and global cooling at this period. We
 537 show that the addition of dust in the atmosphere results in an almost generalized increase
 538 in primary productivity (due to an increase in nutrients availability) in the ocean, but with
 539 a rather heterogeneous spatial distribution. Major productivity increases are located in
 540 areas bordering major deserts, such as in the tropical Atlantic ocean. Some areas, such as
 541 the EEP, show a decrease in primary productivity in response to an increase in dust that
 542 we relate to the supply of non-consumed nutrients. On the other hand, decreasing $p\text{CO}_2$
 543 in the simulations leads to an overall decrease in primary productivity in the ocean, with
 544 again an heterogeneous spatial distribution of anomalies. This is mainly due to the reduced
 545 supply of nutrients from the degradation of organic matter, which is less efficient at lower
 546 temperatures. In addition, we simulated an increase in carbon export to the ocean almost
 547 everywhere, due to the increase in dust. We suggest here that this phenomenon can be linked
 548 to the onset of LMBB, which corresponds to a calcite increase in the sediments and coincides
 549 temporally with a phase of increased dust deposition according to the literature. In a similar
 550 way, the decline in carbon export simulated in response to a decrease in atmospheric $p\text{CO}_2$
 551 levels can be linked to the decline of the LMBB. The heterogeneous pattern of the spatial
 552 distribution of carbon export anomalies is consistent with the heterogeneous pattern of the
 553 LMBB data compilation from Pillot et al. (2023). In order to get a more comprehensive
 554 view of the causes of LMBB onset and decline, further simulations need to include changes
 555 in ocean circulation that occurred in the Late Miocene and Pliocene, as well as changes in
 556 nutrient inputs from rivers. But disentangling all triggering parameters might be difficult.

557 6 Open Research

558 LMDZ, XIOS, NEMO and ORCHIDEE are released under the terms of the CeCILL
 559 license. OASIS-MCT is released under the terms of the Lesser GNU General Public License
 560 (LGPL). IPSL-CM5A2 source code is publicly available through Pillot (2022) The mod.def
 561 file provides information regarding the different revisions used, namely:

- 562 • NEMOGCM branch `nemo_v3_6_STABLE` revision 6665
- 563 • XIOS2 branches/xios-2.5 revision 1763
- 564 • IOIPSL/src svn `tags/v2_2_2`
- 565 • LMDZ5 branches/IPSLCM5A2.1 rev 3591
- 566 • branches/publications/ORCHIDEE IPSL5A2.1.r5307 rev 6336
- 567 • OASIS3-MCT 2.0 branch (rev 4775 IPSL server)

568 We recommend that you refer to the project website: [http://forge.ipsl.jussieu](http://forge.ipsl.jussieu.fr/igcmgdoc/wiki/Doc/Config/IPSLCM5A2)
 569 [.fr/igcmgdoc/wiki/Doc/Config/IPSLCM5A2](http://forge.ipsl.jussieu.fr/igcmgdoc/wiki/Doc/Config/IPSLCM5A2) for a proper installation and compilation of
 570 the environment.

571 All model outputs used in this study that do not come from Sarr et al. (2022) or
 572 Martinot et al. (2022) are available on the repository Pillot (2023).

Acknowledgments

We thank the CEA/ CCRT for providing access to the HPC resources of TGCC under the allocations 2021-A0110102212 and 2022-A0090102212 made by GENCI. This research was funded by the French ANR project MioCarb awarded to BSM (ANR-20-CE49-0002). A-C. Sarr is supported by a grant from Labex OSUG (Investissements d’avenir – ANR10 LABX56). The authors thank Jean-Baptiste Ladant and Marie Laugié for their help in using PISCES-v2 model. Colored maps and 2D profiles in this paper were made with perceptually uniform, color-vision-deficiency-friendly scientific color maps, developed and distributed by F. Crameri (www.fabiocrameri.ch/colourmaps, Crameri et al. (2020)).

References

- Abell, J. T., Rahimi, S. R., Pullen, A., Lebo, Z. J., Zhang, D., Kapp, P., ... Winckler, G. (2020). A Quantitative Model-Based Assessment of Stony Desert Landscape Evolution in the Hami Basin, China: Implications for Plio-Pleistocene Dust Production in Eastern Asia. *Geophysical Research Letters*, *47*(20), e2020GL090064. Retrieved 2023-08-04, from <https://onlinelibrary.wiley.com/doi/abs/10.1029/2020GL090064> (_eprint: <https://agupubs.onlinelibrary.wiley.com/doi/pdf/10.1029/2020GL090064>) doi: 10.1029/2020GL090064
- Abell, J. T., & Winckler, G. (2023). Long-Term Variability in Pliocene North Pacific Ocean Export Production and Its Implications for Ocean Circulation in a Warmer World. *AGU Advances*, *4*(4), e2022AV000853. Retrieved 2023-08-23, from <https://onlinelibrary.wiley.com/doi/abs/10.1029/2022AV000853> (_eprint: <https://agupubs.onlinelibrary.wiley.com/doi/pdf/10.1029/2022AV000853>) doi: 10.1029/2022AV000853
- Andrae, J. W., McInerney, F. A., Polissar, P. J., Sniderman, J. M. K., Howard, S., Hall, P. A., & Phelps, S. R. (2018). Initial Expansion of C4 Vegetation in Australia During the Late Pliocene. *Geophysical Research Letters*, *45*(10), 4831–4840. Retrieved 2023-07-26, from <https://onlinelibrary.wiley.com/doi/abs/10.1029/2018GL077833> (_eprint: <https://agupubs.onlinelibrary.wiley.com/doi/pdf/10.1029/2018GL077833>) doi: 10.1029/2018GL077833
- Aumont, O., & Bopp, L. (2006). Globalizing results from ocean in situ iron fertilization studies. *Global Biogeochemical Cycles*, *20*(2). Retrieved 2023-08-07, from <https://onlinelibrary.wiley.com/doi/abs/10.1029/2005GB002591> (_eprint: <https://agupubs.onlinelibrary.wiley.com/doi/pdf/10.1029/2005GB002591>) doi: 10.1029/2005GB002591
- Aumont, O., Ethé, C., Tagliabue, A., Bopp, L., & Gehlen, M. (2015, August). PISCES-v2: an ocean biogeochemical model for carbon and ecosystem studies. *Geoscientific Model Development*, *8*(8), 2465–2513. Retrieved 2022-01-03, from <https://gmd.copernicus.org/articles/8/2465/2015/> doi: 10.5194/gmd-8-2465-2015
- Aumont, O., Maier-Reimer, E., Blain, S., & Monfray, P. (2003). An ecosystem model of the global ocean including Fe, Si, P colimitations. *Global Biogeochemical Cycles*, *17*(2). Retrieved 2023-08-07, from <https://onlinelibrary.wiley.com/doi/abs/10.1029/2001GB001745> (_eprint: <https://agupubs.onlinelibrary.wiley.com/doi/pdf/10.1029/2001GB001745>) doi: 10.1029/2001GB001745
- Balch, W. M. (2004). Re-evaluation of the physiological ecology of coccolithophores. In H. R. Thierstein & J. R. Young (Eds.), *Coccolithophores: From Molecular Processes to Global Impact* (pp. 165–190). Berlin, Heidelberg: Springer. Retrieved 2023-08-15, from https://doi.org/10.1007/978-3-662-06278-4_7 doi: 10.1007/978-3-662-06278-4_7
- Balkanski, Y., Schulz, M., Claquin, T., Moulin, C., & Ginoux, P. (2004). Global Emissions of Mineral Aerosol: Formulation and Validation using Satellite Imagery. In M. Beniston, C. Granier, P. Artaxo, & C. E. Reeves (Eds.), *Emissions of Atmospheric Trace Compounds* (Vol. 18, pp. 239–267). Dordrecht: Springer Netherlands. Retrieved

- 2023-08-04, from http://link.springer.com/10.1007/978-1-4020-2167-1_6 (Series Title: Advances in Global Change Research) doi: 10.1007/978-1-4020-2167-1_6
- Banerjee, P., & Prasanna Kumar, S. (2014). Dust-induced episodic phytoplankton blooms in the Arabian Sea during winter monsoon. *Journal of Geophysical Research: Oceans*, 119(10), 7123–7138. Retrieved 2023-07-31, from <https://onlinelibrary.wiley.com/doi/abs/10.1002/2014JC010304> (eprint: <https://agupubs.onlinelibrary.wiley.com/doi/pdf/10.1002/2014JC010304>) doi: 10.1002/2014JC010304
- Beaufort, L., Bolton, C. T., Sarr, A.-C., Suchéras-Marx, B., Rosenthal, Y., Donnadiou, Y., ... Tetard, M. (2022, January). Cyclic evolution of phytoplankton forced by changes in tropical seasonality. *Nature*, 601(7891), 79–84. Retrieved 2023-09-05, from <https://www.nature.com/articles/s41586-021-04195-7> doi: 10.1038/s41586-021-04195-7
- Behrenfeld, M. J., O'Malley, R. T., Siegel, D. A., McClain, C. R., Sarmiento, J. L., Feldman, G. C., ... Boss, E. S. (2006, December). Climate-driven trends in contemporary ocean productivity. *Nature*, 444(7120), 752–755. Retrieved 2023-07-31, from <https://www.nature.com/articles/nature05317> doi: 10.1038/nature05317
- Bendtsen, J., Hilligsøe, K. M., Hansen, J. L., & Richardson, K. (2015, January). Analysis of remineralisation, lability, temperature sensitivity and structural composition of organic matter from the upper ocean. *Progress in Oceanography*, 130, 125–145. Retrieved 2023-07-31, from <https://linkinghub.elsevier.com/retrieve/pii/S0079661114001724> doi: 10.1016/j.pocean.2014.10.009
- Bierman, P. R., Shakun, J. D., Corbett, L. B., Zimmerman, S. R., & Rood, D. H. (2016, December). A persistent and dynamic East Greenland Ice Sheet over the past 7.5 million years. *Nature*, 540(7632), 256–260. Retrieved 2020-08-28, from <http://www.nature.com/articles/nature20147> doi: 10.1038/nature20147
- Bolton, C. T., Gray, E., Kuhnt, W., Holbourn, A. E., Lübbers, J., Grant, K., ... Andersen, N. (2022, April). Secular and orbital-scale variability of equatorial Indian Ocean summer monsoon winds during the late Miocene. *Climate of the Past*, 18(4), 713–738. Retrieved 2022-08-15, from <https://cp.copernicus.org/articles/18/713/2022/> doi: 10.5194/cp-18-713-2022
- Bopp, L., Kohfeld, K. E., Le Quééré, C., & Aumont, O. (2003). Dust impact on marine biota and atmospheric CO₂ during glacial periods. *Paleoceanography*, 18(2). Retrieved 2023-04-25, from <https://onlinelibrary.wiley.com/doi/abs/10.1029/2002PA000810> (eprint: <https://agupubs.onlinelibrary.wiley.com/doi/pdf/10.1029/2002PA000810>) doi: 10.1029/2002PA000810
- Brierley, C. M., & Fedorov, A. V. (2016, June). Comparing the impacts of Miocene–Pliocene changes in inter-ocean gateways on climate: Central American Seaway, Bering Strait, and Indonesia. *Earth and Planetary Science Letters*, 444, 116–130. Retrieved 2021-05-10, from <https://linkinghub.elsevier.com/retrieve/pii/S0012821X16300978> doi: 10.1016/j.epsl.2016.03.010
- Buitenhuis, E. T., Hashioka, T., & Quééré, C. L. (2013). Combined constraints on global ocean primary production using observations and models. *Global Biogeochemical Cycles*, 27(3), 847–858. Retrieved 2023-08-22, from <https://onlinelibrary.wiley.com/doi/abs/10.1002/gbc.20074> (eprint: <https://agupubs.onlinelibrary.wiley.com/doi/pdf/10.1002/gbc.20074>) doi: 10.1002/gbc.20074
- Burls, N. J., Bradshaw, C., De Boer, A. M., Herold, N., Huber, M., Pound, M., ... Zhang, Z. (2021, January). *Simulating Miocene warmth: insights from an opportunistic Multi-Model ensemble (MioMIP1)* (preprint). *Climatology (Global Change)*. Retrieved 2021-05-06, from <http://www.essoar.org/doi/10.1002/essoar.10505870.1> doi: 10.1002/essoar.10505870.1
- Burls, N. J., Fedorov, A. V., Sigman, D. M., Jaccard, S. L., Tiedemann, R., & Haug, G. H. (2017, September). Active Pacific meridional overturning circulation (PMOC) during the warm Pliocene. *Science Advances*, 3(9), e1700156. Retrieved 2023-08-23, from <https://www.science.org/doi/10.1126/sciadv.1700156> doi: 10.1126/

- 681 sciadv.1700156
- 682 Cabré, A., Marinov, I., & Leung, S. (2015, September). Consistent global responses of
 683 marine ecosystems to future climate change across the IPCC AR5 earth system models.
 684 *Climate Dynamics*, 45(5-6), 1253–1280. Retrieved 2023-08-08, from [http://link](http://link.springer.com/10.1007/s00382-014-2374-3)
 685 [.springer.com/10.1007/s00382-014-2374-3](http://link.springer.com/10.1007/s00382-014-2374-3) doi: 10.1007/s00382-014-2374-3
- 686 Cerling, T. E., Harris, J. M., MacFadden, B. J., Leakey, M. G., Quade, J., Eisenmann,
 687 V., & Ehleringer, J. R. (1997, September). Global vegetation change through the
 688 Miocene/Pliocene boundary. *Nature*, 389(6647), 153–158. Retrieved 2022-09-22, from
 689 <http://www.nature.com/articles/38229> doi: 10.1038/38229
- 690 Clift, P. D., Kulhanek, D. K., Zhou, P., Bowen, M. G., Vincent, S. M., Lyle, M., & Hahn, A.
 691 (2020, June). Chemical weathering and erosion responses to changing monsoon climate
 692 in the Late Miocene of Southwest Asia. *Geological Magazine*, 157(6), 939–955. Re-
 693 trieved 2022-07-20, from [https://www.cambridge.org/core/product/identifier/](https://www.cambridge.org/core/product/identifier/S0016756819000608/type/journal_article)
 694 [S0016756819000608/type/journal_article](https://www.cambridge.org/core/product/identifier/S0016756819000608/type/journal_article) doi: 10.1017/S0016756819000608
- 695 Cortese, G., Gersonde, R., Hillenbrand, C.-D., & Kuhn, G. (2004, August). Opal sedimenta-
 696 tion shifts in the World Ocean over the last 15 Myr. *Earth and Planetary Science Let-*
 697 *ters*, 224(3-4), 509–527. Retrieved 2020-11-09, from [https://linkinghub.elsevier](https://linkinghub.elsevier.com/retrieve/pii/S0012821X04003553)
 698 [.com/retrieve/pii/S0012821X04003553](https://linkinghub.elsevier.com/retrieve/pii/S0012821X04003553) doi: 10.1016/j.epsl.2004.05.035
- 699 Cramer, F., Shephard, G. E., & Heron, P. J. (2020, December). The misuse of colour
 700 in science communication. *Nature Communications*, 11(1), 5444. Retrieved 2022-05-
 701 26, from <http://www.nature.com/articles/s41467-020-19160-7> doi: 10.1038/
 702 [s41467-020-19160-7](http://www.nature.com/articles/s41467-020-19160-7)
- 703 Crichton, K. A., Wilson, J. D., Ridgwell, A., & Pearson, P. N. (2021, January). Cal-
 704 ibration of temperature-dependent ocean microbial processes in the cGENIE.muffin
 705 (v0.9.13) Earth system model. *Geoscientific Model Development*, 14(1), 125–149.
 706 Retrieved 2023-06-27, from <https://gmd.copernicus.org/articles/14/125/2021/>
 707 (Publisher: Copernicus GmbH) doi: 10.5194/gmd-14-125-2021
- 708 Crocker, A. J., Naafs, B. D. A., Westerhold, T., James, R. H., Cooper, M. J., Röhl, U., ...
 709 Wilson, P. A. (2022, July). Astronomically controlled aridity in the Sahara since at
 710 least 11 million years ago. *Nature Geoscience*. Retrieved 2022-07-26, from [https://](https://www.nature.com/articles/s41561-022-00990-7)
 711 www.nature.com/articles/s41561-022-00990-7 doi: 10.1038/s41561-022-00990-7
- 712 Curry, WB and Shackleton, NJ and Richter, C and Backman, JE and Bassinot, F and
 713 Bickert, T and Chaisson, WP and Cullen, JL and deMenocal, P and Dobson, DM and
 714 others. (1995). Leg synthesis. *Proceedings Ocean Drilling Program, Initial Reports*
 715 *155*, 17–21. (Publisher: Ocean Drilling Program)
- 716 Dansie, A., Thomas, D., Wiggs, G., Baddock, M., & Ashpole, I. (2022, July). Plumes and
 717 blooms – Locally-sourced Fe-rich aeolian mineral dust drives phytoplankton growth off
 718 southwest Africa. *Science of The Total Environment*, 829, 154562. Retrieved 2023-07-
 719 27, from <https://linkinghub.elsevier.com/retrieve/pii/S0048969722016552>
 720 doi: 10.1016/j.scitotenv.2022.154562
- 721 Davini, P., von Hardenberg, J., Filippi, L., & Provenzale, A. (2015, February). Impact of
 722 Greenland orography on the Atlantic Meridional Overturning Circulation. *Geophysical*
 723 *Research Letters*, 42(3), 871–879. Retrieved 2020-08-28, from [http://doi.wiley](http://doi.wiley.com/10.1002/2014GL062668)
 724 [.com/10.1002/2014GL062668](http://doi.wiley.com/10.1002/2014GL062668) doi: 10.1002/2014GL062668
- 725 de la Vega, E., Chalk, T. B., Wilson, P. A., Bysani, R. P., & Foster, G. L. (2020, July).
 726 Atmospheric CO₂ during the Mid-Piacenzian Warm Period and the M2 glaciation.
 727 *Scientific Reports*, 10, 11002. Retrieved 2023-08-15, from [https://www.ncbi.nlm](https://www.ncbi.nlm.nih.gov/pmc/articles/PMC7347535/)
 728 [.nih.gov/pmc/articles/PMC7347535/](https://www.ncbi.nlm.nih.gov/pmc/articles/PMC7347535/) doi: 10.1038/s41598-020-67154-8
- 729 del Giorgio, P. A., & Duarte, C. M. (2002, November). Respiration in the open ocean.
 730 *Nature*, 420(6914), 379–384. Retrieved 2023-07-31, from [https://www.nature.com/](https://www.nature.com/articles/nature01165)
 731 [articles/nature01165](https://www.nature.com/articles/nature01165) doi: 10.1038/nature01165
- 732 Dickens, G. R., & Owen, R. M. (1999, September). The Latest Miocene–Early Pliocene
 733 biogenic bloom: a revised Indian Ocean perspective. *Marine Geology*, 161(1), 75–
 734 91. Retrieved 2020-11-09, from [https://linkinghub.elsevier.com/retrieve/pii/](https://linkinghub.elsevier.com/retrieve/pii/S0025322799000572)
 735 [S0025322799000572](https://linkinghub.elsevier.com/retrieve/pii/S0025322799000572) doi: 10.1016/S0025-3227(99)00057-2

- 736 Diester-Haass, L., Billups, K., & Emeis, K. C. (2005). In search of the late Miocene–early
737 Pliocene “biogenic bloom” in the Atlantic Ocean (Ocean Drilling Program Sites
738 982, 925, and 1088). *Paleoceanography*, *20*(4). Retrieved 2022-03-15, from
739 <http://onlinelibrary.wiley.com/doi/abs/10.1029/2005PA001139> (eprint:
740 <https://agupubs.onlinelibrary.wiley.com/doi/pdf/10.1029/2005PA001139>) doi: 10
741 .1029/2005PA001139
- 742 Diester-Haass, L., Billups, K., & Emeis, K. C. (2006). Late Miocene
743 carbon isotope records and marine biological productivity: Was there a
744 (dusty) link? *Paleoceanography*, *21*(4). Retrieved 2022-03-15, from
745 <http://onlinelibrary.wiley.com/doi/abs/10.1029/2006PA001267> (eprint:
746 <https://agupubs.onlinelibrary.wiley.com/doi/pdf/10.1029/2006PA001267>) doi: 10
747 .1029/2006PA001267
- 748 Drury, A. J., Liebrand, D., Westerhold, T., Beddow, H. M., Hodell, D. A., Rohlfs, N.,
749 ... Lourens, L. J. (2021, October). Climate, cryosphere and carbon cycle controls
750 on Southeast Atlantic orbital-scale carbonate deposition since the Oligocene (30–0
751 Ma). *Climate of the Past*, *17*(5), 2091–2117. Retrieved 2022-03-03, from [https://](https://cp.copernicus.org/articles/17/2091/2021/)
752 cp.copernicus.org/articles/17/2091/2021/ doi: 10.5194/cp-17-2091-2021
- 753 Dufresne, J.-L., Foujols, M.-A., Denvil, S., Caubel, A., Marti, O., Aumont, O., ... Vuichard,
754 N. (2013, May). Climate change projections using the IPSL-CM5 Earth System
755 Model: from CMIP3 to CMIP5. *Climate Dynamics*, *40*(9-10), 2123–2165. Retrieved
756 2022-01-03, from <http://link.springer.com/10.1007/s00382-012-1636-1> doi:
757 10.1007/s00382-012-1636-1
- 758 Dutkiewicz, S., Follows, M. J., & Parekh, P. (2005). Interactions of the
759 iron and phosphorus cycles: A three-dimensional model study. *Global*
760 *Biogeochemical Cycles*, *19*(1). Retrieved 2023-08-07, from [https://](https://onlinelibrary.wiley.com/doi/abs/10.1029/2004GB002342)
761 onlinelibrary.wiley.com/doi/abs/10.1029/2004GB002342 (eprint:
762 <https://agupubs.onlinelibrary.wiley.com/doi/pdf/10.1029/2004GB002342>) doi:
763 10.1029/2004GB002342
- 764 Farley, K. A., Vokrouhlický, D., Bottke, W. F., & Nesvorný, D. (2006, January). A
765 late Miocene dust shower from the break-up of an asteroid in the main belt. *Nature*,
766 *439*(7074), 295–297. Retrieved 2023-06-28, from [https://www.nature.com/](https://www.nature.com/articles/nature04391)
767 [articles/nature04391](https://www.nature.com/articles/nature04391) doi: 10.1038/nature04391
- 768 Farrell, J. W., Raffi, I., Janecek, T. R., Murray, D. W., Levitan, M., Dadey, K. A., ...
769 Hovan, S. (1995). 35. LATE NEOGENE SEDIMENTATION PATTERNS IN THE
770 EASTERN EQUATORIAL PACIFIC OCEAN. , 40.
- 771 Feakins, S. J., Levin, N. E., Liddy, H. M., Sieracki, A., Eglinton, T. I., & Bonnefille,
772 R. (2013, March). Northeast African vegetation change over 12 m.y. *Geology*,
773 *41*(3), 295–298. Retrieved 2023-07-26, from [https://pubs.geoscienceworld.org/](https://pubs.geoscienceworld.org/geology/article/41/3/295-298/131095)
774 [geology/article/41/3/295-298/131095](https://pubs.geoscienceworld.org/geology/article/41/3/295-298/131095) doi: 10.1130/G33845.1
- 775 Field, C. B., Behrenfeld, M. J., Randerson, J. T., & Falkowski, P. (1998, July). Primary
776 Production of the Biosphere: Integrating Terrestrial and Oceanic Components. *Sci-*
777 *ence*, *281*(5374), 237–240. Retrieved 2023-10-13, from [https://www.science.org/](https://www.science.org/doi/10.1126/science.281.5374.237)
778 [doi/10.1126/science.281.5374.237](https://www.science.org/doi/10.1126/science.281.5374.237) doi: 10.1126/science.281.5374.237
- 779 Filippelli, G. M. (1997). Intensification of the Asian monsoon and a chemical weathering
780 event in the late Miocene–early Pliocene: Implications for late Neogene climate change.
781 , 4.
- 782 Ford, H. L., Burls, N. J., Jacobs, P., Jahn, A., Caballero-Gill, R. P., Hodell, D. A., &
783 Fedorov, A. V. (2022, August). Sustained mid-Pliocene warmth led to deep water
784 formation in the North Pacific. *Nature Geoscience*, *15*(8), 658–663. Retrieved 2023-08-
785 23, from <https://www.nature.com/articles/s41561-022-00978-3> doi: 10.1038/
786 s41561-022-00978-3
- 787 Fujioka, T., Chappell, J., Fifield, L. K., & Rhodes, E. J. (2009, January). Australian desert
788 dune fields initiated with Pliocene–Pleistocene global climatic shift. *Geology*, *37*(1),
789 51–54. Retrieved 2023-08-18, from [http://pubs.geoscienceworld.org/geology/](http://pubs.geoscienceworld.org/geology/article/37/1/51/193509/Australian-desert-dune-fields-initiated-with)
790 [article/37/1/51/193509/Australian-desert-dune-fields-initiated-with](http://pubs.geoscienceworld.org/geology/article/37/1/51/193509/Australian-desert-dune-fields-initiated-with)

- 791 doi: 10.1130/G25042A.1
- 792 Gastaldello, M. E., Agnini, C., Westerhold, T., Drury, A. J., Sutherland, R.,
793 Drake, M. K., ... Alegret, L. (2023). The Late Miocene-Early Pliocene
794 Biogenic Bloom: An Integrated Study in the Tasman Sea. *Paleoceanogra-*
795 *phy and Paleoclimatology*, 38(4), e2022PA004565. Retrieved 2023-04-06, from
796 <https://onlinelibrary.wiley.com/doi/abs/10.1029/2022PA004565> (eprint:
797 <https://agupubs.onlinelibrary.wiley.com/doi/pdf/10.1029/2022PA004565>) doi: 10
798 .1029/2022PA004565
- 799 Gladenkov, A. Y., & Gladenkov, Y. B. (2004). Onset of Connections between the Pacific
800 and Arctic Oceans through the Bering Strait in the Neogene. , 12(2), 13.
- 801 Grant, K. M., & Dickens, G. R. (2002). Coupled productivity and carbon isotope records in
802 the southwest Pacific Ocean during the late Miocene-early Pliocene biogenic bloom. ,
803 22.
- 804 Gupta, A. K., Singh, R. K., Joseph, S., & Thomas, E. (2004). Indian Ocean high-
805 productivity event (10–8 Ma): Linked to global cooling or to the initiation of the
806 Indian monsoons? *Geology*, 32(9), 753. Retrieved 2020-11-09, from [https://pubs](https://pubs.geoscienceworld.org/geology/article/32/9/753-756/103705)
807 [.geoscienceworld.org/geology/article/32/9/753-756/103705](https://pubs.geoscienceworld.org/geology/article/32/9/753-756/103705) doi: 10.1130/
808 G20662.1
- 809 Hall, J. R., Allison, M. S., Papadopoulos, M. T., Barfod, D. N., & Jones, S. M. (2023, April).
810 Timing and Consequences of Bering Strait Opening: New Insights From 40Ar/39Ar
811 Dating of the Barmur Group (Tjörnes Beds), Northern Iceland. *Paleoceanography*
812 *and Paleoclimatology*, 38(4), e2022PA004539. Retrieved 2023-09-27, from [https://](https://agupubs.onlinelibrary.wiley.com/doi/10.1029/2022PA004539)
813 agupubs.onlinelibrary.wiley.com/doi/10.1029/2022PA004539 (Publisher: John
814 Wiley & Sons, Ltd) doi: 10.1029/2022PA004539
- 815 Haywood, A. M., Tindall, J. C., Dowsett, H. J., Dolan, A. M., Foley, K. M., Hunter, S. J., ...
816 Lunt, D. J. (2020, November). The Pliocene Model Intercomparison Project Phase
817 2: large-scale climate features and climate sensitivity. *Climate of the Past*, 16(6),
818 2095–2123. Retrieved 2023-10-14, from [https://cp.copernicus.org/articles/16/](https://cp.copernicus.org/articles/16/2095/2020/)
819 [2095/2020/](https://cp.copernicus.org/articles/16/2095/2020/) (Publisher: Copernicus GmbH) doi: 10.5194/cp-16-2095-2020
- 820 Herbert, T. D., Lawrence, K. T., Tzanova, A., Peterson, L. C., Caballero-Gill, R., &
821 Kelly, C. S. (2016, November). Late Miocene global cooling and the rise of mod-
822 ern ecosystems. *Nature Geoscience*, 9(11), 843–847. Retrieved 2020-11-09, from
823 <http://www.nature.com/articles/ngeo2813> doi: 10.1038/ngeo2813
- 824 Hermoyian, C. S., & Owen, R. M. (2001). Late Miocene-early Pliocene bio-
825 genic bloom: Evidence from low-productivity regions of the Indian and At-
826 lantic Oceans. *Paleoceanography*, 16(1), 95–100. Retrieved 2022-03-15, from
827 <http://onlinelibrary.wiley.com/doi/abs/10.1029/2000PA000501> (eprint:
828 <https://agupubs.onlinelibrary.wiley.com/doi/pdf/10.1029/2000PA000501>) doi: 10
829 .1029/2000PA000501
- 830 Herold, N., Huber, M., & Müller, R. D. (2011, December). Modeling the Miocene Cli-
831 matic Optimum. Part I: Land and Atmosphere*. *Journal of Climate*, 24(24), 6353–
832 6372. Retrieved 2021-08-31, from [http://journals.ametsoc.org/doi/10.1175/](http://journals.ametsoc.org/doi/10.1175/2011JCLI4035.1)
833 [2011JCLI4035.1](http://journals.ametsoc.org/doi/10.1175/2011JCLI4035.1) doi: 10.1175/2011JCLI4035.1
- 834 Herold, N., Huber, M., Müller, R. D., & Seton, M. (2012, March). Modeling the
835 Miocene climatic optimum: Ocean circulation: MODELING MIOCENE OCEAN
836 CIRCULATION. *Paleoceanography*, 27(1), n/a–n/a. Retrieved 2020-08-28, from
837 <http://doi.wiley.com/10.1029/2010PA002041> doi: 10.1029/2010PA002041
- 838 Holbourn, A. E., Kuhnt, W., Clemens, S. C., Kochhann, K. G. D., Jöhnck, J., Lübbers, J.,
839 & Andersen, N. (2018, December). Late Miocene climate cooling and intensification
840 of southeast Asian winter monsoon. *Nature Communications*, 9(1), 1584. Retrieved
841 2022-07-20, from <http://www.nature.com/articles/s41467-018-03950-1> doi: 10
842 .1038/s41467-018-03950-1
- 843 Hooper, J., Mayewski, P., Marx, S., Henson, S., Potocki, M., Sneed, S., ... Saunders,
844 K. M. (2019, February). Examining links between dust deposition and phytoplankton
845 response using ice cores. *Aeolian Research*, 36, 45–60. Retrieved 2023-07-26, from

- 846 <https://linkinghub.elsevier.com/retrieve/pii/S1875963718301101> doi: 10
847 .1016/j.aeolia.2018.11.001
- 848 Hossain, A., Knorr, G., Jokat, W., Lohmann, G., Hochmuth, K., Gierz, P.,
849 ... Stepanek, C. (2023). The Impact of Different Atmospheric CO₂ Con-
850 centrations on Large Scale Miocene Temperature Signatures. *Paleoceanogra-
851 phy and Paleoclimatology*, 38(2), e2022PA004438. Retrieved 2023-06-28, from
852 <https://onlinelibrary.wiley.com/doi/abs/10.1029/2022PA004438> (eprint:
853 <https://agupubs.onlinelibrary.wiley.com/doi/pdf/10.1029/2022PA004438>) doi: 10
854 .1029/2022PA004438
- 855 Hossain, A., Knorr, G., Lohmann, G., Stürz, M., & Jokat, W. (2020, July). Simulated
856 Thermohaline Fingerprints in Response to Different Greenland-Scotland Ridge and
857 Fram Strait Subsidence Histories. *Paleoceanography and Paleoclimatology*, 35(7).
858 Retrieved 2021-05-10, from [https://onlinelibrary.wiley.com/doi/abs/10.1029/
859 2019PA003842](https://onlinelibrary.wiley.com/doi/abs/10.1029/2019PA003842) doi: 10.1029/2019PA003842
- 860 Hourdin, F., Foujols, M.-A., Codron, F., Guemas, V., Dufresne, J.-L., Bony, S., ... Bopp,
861 L. (2013, May). Impact of the LMDZ atmospheric grid configuration on the climate
862 and sensitivity of the IPSL-CM5A coupled model. *Climate Dynamics*, 40(9-10), 2167–
863 2192. Retrieved 2022-01-03, from [http://link.springer.com/10.1007/s00382-012-
864 -1411-3](http://link.springer.com/10.1007/s00382-012-1411-3) doi: 10.1007/s00382-012-1411-3
- 865 Hovan, S. A. (1995). 28. Late Cenozoic atmospheric circulation intensity and climatic
866 history recorded by Eolian deposition in the Eastern Equatorial Pacific Ocean, Leg
867 138. *Proceedings of the Ocean Drilling Program, Scientific Results. Proceedings of the
868 Ocean Drilling Program, Scientific Results*, 615–625.
- 869 Jickells, T., & Moore, C. M. (2015, December). The Importance of Atmospheric Deposi-
870 tion for Ocean Productivity. *Annual Review of Ecology, Evolution, and Systematics*,
871 46(1), 481–501. Retrieved 2023-07-26, from [https://www.annualreviews.org/doi/
872 10.1146/annurev-ecolsys-112414-054118](https://www.annualreviews.org/doi/10.1146/annurev-ecolsys-112414-054118) doi: 10.1146/annurev-ecolsys-112414
873 -054118
- 874 Jickells, T. D., An, Z. S., Andersen, K. K., Baker, A. R., Bergametti, G., Brooks, N.,
875 ... Torres, R. (2005, April). Global Iron Connections Between Desert Dust, Ocean
876 Biogeochemistry, and Climate. *Science*, 308(5718), 67–71. Retrieved 2023-07-25, from
877 <https://www.science.org/doi/10.1126/science.1105959> doi: 10.1126/science
878 .1105959
- 879 Kamae, Y., Ueda, H., & Kitoh, A. (2011). Hadley and Walker Circulations in the Mid-
880 Pliocene Warm Period Simulated by an Atmospheric General Circulation Model. *Jour-
881 nal of the Meteorological Society of Japan. Ser. II*, 89(5), 475–493. Retrieved 2022-09-
882 26, from http://www.jstage.jst.go.jp/article/jmsj/89/5/89_5_475/_article
883 doi: 10.2151/jmsj.2011-505
- 884 Karatsolis, B. ., Lougheed, B. C., De Vleeschouwer, D., & Henderiks, J. (2022, Decem-
885 ber). Abrupt conclusion of the late Miocene-early Pliocene biogenic bloom at 4.6-
886 4.4 Ma. *Nature Communications*, 13(1), 353. Retrieved 2022-01-25, from [https://
887 www.nature.com/articles/s41467-021-27784-6](https://www.nature.com/articles/s41467-021-27784-6) doi: 10.1038/s41467-021-27784-6
- 888 Krinner, G., Viovy, N., de Noblet-Ducoudré, N., Ogée, J., Polcher, J., Friedlingstein, P.,
889 ... Prentice, I. C. (2005, March). A dynamic global vegetation model for studies
890 of the coupled atmosphere-biosphere system: DVGM FOR COUPLED CLIMATE
891 STUDIES. *Global Biogeochemical Cycles*, 19(1). Retrieved 2022-01-03, from [http://
892 doi.wiley.com/10.1029/2003GB002199](http://doi.wiley.com/10.1029/2003GB002199) doi: 10.1029/2003GB002199
- 893 Kuhnt, W., Holbourn, A., Hall, R., Zuvela, M., & Käse, R. (2004). Neogene History
894 of the Indonesian Throughflow. In *Continent-Ocean Interactions Within East Asian
895 Marginal Seas* (pp. 299–320). American Geophysical Union (AGU). Retrieved 2022-09-
896 22, from <http://onlinelibrary.wiley.com/doi/abs/10.1029/149GM16> (eprint:
897 <https://agupubs.onlinelibrary.wiley.com/doi/pdf/10.1029/149GM16>) doi: 10.1029/
898 149GM16
- 899 Kwiatkowski, L., Aumont, O., & Bopp, L. (2019). Consistent trophic amplification of ma-
900 rine biomass declines under climate change. *Global Change Biology*, 25(1), 218–229.

- Retrieved 2023-04-21, from <https://onlinelibrary.wiley.com/doi/abs/10.1111/gcb.14468> (eprint: <https://onlinelibrary.wiley.com/doi/pdf/10.1111/gcb.14468>) doi: 10.1111/gcb.14468
- 901
902
903
- 904 Ladant, J.-B., Donnadiou, Y., Bopp, L., Lear, C. H., & Wilson, P. A. (2018, March).
905 Meridional Contrasts in Productivity Changes Driven by the Opening of Drake Pas-
906 sage. *Paleoceanography and Paleoclimatology*, *33*(3), 302–317. Retrieved 2020-08-28,
907 from <http://doi.wiley.com/10.1002/2017PA003211> doi: 10.1002/2017PA003211
- 908 Lambert, F., Tagliabue, A., Shaffer, G., Lamy, F., Winckler, G., Farias, L., ... De Pol-Holz,
909 R. (2015). Dust fluxes and iron fertilization in Holocene and Last Glacial Maximum cli-
910 mates. *Geophysical Research Letters*, *42*(14), 6014–6023. Retrieved 2023-06-28, from
911 <https://onlinelibrary.wiley.com/doi/abs/10.1002/2015GL064250> (eprint:
912 <https://agupubs.onlinelibrary.wiley.com/doi/pdf/10.1002/2015GL064250>) doi: 10
913 .1002/2015GL064250
- 914 Laufkötter, C., Vogt, M., Gruber, N., Aita-Noguchi, M., Aumont, O., Bopp, L., ... Völker,
915 C. (2015, December). Drivers and uncertainties of future global marine primary
916 production in marine ecosystem models. *Biogeosciences*, *12*(23), 6955–6984. Re-
917 trieved 2023-08-22, from [https://bg.copernicus.org/articles/12/6955/2015/bg-](https://bg.copernicus.org/articles/12/6955/2015/bg-12-6955-2015.html)
918 [12-6955-2015.html](https://bg.copernicus.org/articles/12/6955/2015/bg-12-6955-2015.html) (Publisher: Copernicus GmbH) doi: 10.5194/bg-12-6955-2015
- 919 Le Mézo, P., Beaufort, L., Bopp, L., Braconnot, P., & Kageyama, M. (2017, July). From
920 monsoon to marine productivity in the Arabian Sea: insights from glacial and inter-
921 terglacial climates. *Climate of the Past*, *13*(7), 759–778. Retrieved 2023-09-05,
922 from <https://cp.copernicus.org/articles/13/759/2017/cp-13-759-2017.html>
923 (Publisher: Copernicus GmbH) doi: 10.5194/cp-13-759-2017
- 924 Lohmann, G., Knorr, G., Hossain, A., & Stepanek, C. (2022). Effects of CO₂ and
925 Ocean Mixing on Miocene and Pliocene Temperature Gradients. *Paleoceanog-*
926 *raphy and Paleoclimatology*, *37*(2), e2020PA003953. Retrieved 2023-02-14, from
927 <https://onlinelibrary.wiley.com/doi/abs/10.1029/2020PA003953> (eprint:
928 <https://agupubs.onlinelibrary.wiley.com/doi/pdf/10.1029/2020PA003953>) doi: 10
929 .1029/2020PA003953
- 930 Lyle, M., & Baldauf, J. (2015, September). Biogenic sediment regimes in the Neogene equa-
931 torial Pacific, IODP Site U1338: Burial, production, and diatom community. *Palaeo-*
932 *geography, Palaeoclimatology, Palaeoecology*, *433*, 106–128. Retrieved 2020-11-09,
933 from <https://linkinghub.elsevier.com/retrieve/pii/S0031018215001868> doi:
934 10.1016/j.palaeo.2015.04.001
- 935 Lyle, M., Drury, A. J., Tian, J., Wilkens, R., & Westerhold, T. (2019, September). Late
936 Miocene to Holocene high-resolution eastern equatorial Pacific carbonate records:
937 stratigraphy linked by dissolution and paleoproductivity. *Climate of the Past*, *15*(5),
938 1715–1739. Retrieved 2021-01-25, from [https://cp.copernicus.org/articles/15/](https://cp.copernicus.org/articles/15/1715/2019/)
939 [1715/2019/](https://cp.copernicus.org/articles/15/1715/2019/) doi: 10.5194/cp-15-1715-2019
- 940 Lyu, J., Auer, G., Bialik, O. M., Christensen, B., Yamaoka, R., & De Vleeschouwer,
941 D. (2023, December). Astronomically-Paced Changes in Paleoproductivity,
942 Winnowing, and Mineral Flux Over Broken Ridge (Indian Ocean) Since the
943 Early Miocene. *Paleoceanography and Paleoclimatology*, *38*(12), e2023PA004761.
944 Retrieved 2023-12-19, from [https://agupubs.onlinelibrary.wiley.com/doi/10](https://agupubs.onlinelibrary.wiley.com/doi/10.1029/2023PA004761)
945 [.1029/2023PA004761](https://agupubs.onlinelibrary.wiley.com/doi/10.1029/2023PA004761) doi: 10.1029/2023PA004761
- 946 López-Urrutia, , San Martin, E., Harris, R. P., & Irigoien, X. (2006, June). Scaling the
947 metabolic balance of the oceans. *Proceedings of the National Academy of Sciences*,
948 *103*(23), 8739–8744. Retrieved 2023-07-31, from [https://pnas.org/doi/full/10](https://pnas.org/doi/full/10.1073/pnas.0601137103)
949 [.1073/pnas.0601137103](https://pnas.org/doi/full/10.1073/pnas.0601137103) doi: 10.1073/pnas.0601137103
- 950 Lübbers, J., Kuhnt, W., Holbourn, A., Bolton, C., Gray, E., Usui, Y., ... Andersen, N.
951 (2019, May). The Middle to Late Miocene “Carbonate Crash” in the Equatorial
952 Indian Ocean. *Paleoceanography and Paleoclimatology*, *34*(5), 813–832. Retrieved
953 2022-09-19, from <https://hal.archives-ouvertes.fr/hal-02341889> (Publisher:
954 American Geophysical Union) doi: 10.1029/2018PA003482
- 955 Madec, G. (2016). NEMO ocean engine. , 396.

- 956 Mahowald, N., Jickells, T. D., Baker, A. R., Artaxo, P., Benitez-Nelson, C. R., Bergametti,
957 G., ... Tsukuda, S. (2008, December). Global distribution of atmospheric phosphorus
958 sources, concentrations and deposition rates, and anthropogenic impacts: GLOBAL
959 ATMOSPHERIC PHOSPHORUS. *Global Biogeochemical Cycles*, 22(4), n/a–n/a.
960 Retrieved 2023-07-25, from <http://doi.wiley.com/10.1029/2008GB003240> doi:
961 10.1029/2008GB003240
- 962 Mahowald, N. M., Baker, A. R., Bergametti, G., Brooks, N., Duce, R. A., Jickells,
963 T. D., ... Tegen, I. (2005). Atmospheric global dust cycle and iron inputs
964 to the ocean. *Global Biogeochemical Cycles*, 19(4). Retrieved 2023-07-31, from
965 <https://onlinelibrary.wiley.com/doi/abs/10.1029/2004GB002402> (eprint:
966 <https://agupubs.onlinelibrary.wiley.com/doi/pdf/10.1029/2004GB002402>) doi: 10
967 .1029/2004GB002402
- 968 Martinot, C., Bolton, C. T., Sarr, A.-C., Donnadieu, Y., Garcia, M., Gray, E., &
969 Tachikawa, K. (2022). Drivers of Late Miocene Tropical Sea Surface Cool-
970 ing: A New Perspective From the Equatorial Indian Ocean. *Paleoceanogra-
971 phy and Paleoclimatology*, 37(10), e2021PA004407. Retrieved 2023-01-11, from
972 <https://onlinelibrary.wiley.com/doi/abs/10.1029/2021PA004407> (eprint:
973 <https://agupubs.onlinelibrary.wiley.com/doi/pdf/10.1029/2021PA004407>) doi: 10
974 .1029/2021PA004407
- 975 Molnar, P. (2008). Closing of the Central American Seaway and the Ice Age:
976 A critical review. *Paleoceanography*, 23(2). Retrieved 2023-09-05, from
977 <https://onlinelibrary.wiley.com/doi/abs/10.1029/2007PA001574> (eprint:
978 <https://agupubs.onlinelibrary.wiley.com/doi/pdf/10.1029/2007PA001574>) doi: 10
979 .1029/2007PA001574
- 980 Molnar, P. (2017, June). Comment (2) on “Formation of the Isthmus of Panama” by O’Dea
981 *et al* . *Science Advances*, 3(6), e1602320. Retrieved 2023-09-05, from [https://](https://www.science.org/doi/10.1126/sciadv.1602320)
982 www.science.org/doi/10.1126/sciadv.1602320 doi: 10.1126/sciadv.1602320
- 983 Montes, C., Cardona, A., Jaramillo, C., Pardo, A., Silva, J. C., Valencia, V., ... Nino, H.
984 (2015, April). Middle Miocene closure of the Central American Seaway. *Science*,
985 348(6231), 226–229. Retrieved 2021-05-10, from [https://www.sciencemag.org/](https://www.sciencemag.org/lookup/doi/10.1126/science.aaa2815)
986 [lookup/doi/10.1126/science.aaa2815](https://www.sciencemag.org/lookup/doi/10.1126/science.aaa2815) doi: 10.1126/science.aaa2815
- 987 Moore, C. M., Mills, M. M., Arrigo, K. R., Berman-Frank, I., Bopp, L., Boyd, P. W., ...
988 Ulloa, O. (2013, September). Processes and patterns of oceanic nutrient limitation.
989 *Nature Geoscience*, 6(9), 701–710. Retrieved 2023-07-27, from [https://www.nature](https://www.nature.com/articles/ngeo1765)
990 [.com/articles/ngeo1765](https://www.nature.com/articles/ngeo1765) doi: 10.1038/ngeo1765
- 991 Moore, J., Doney, S. C., Glover, D. M., & Fung, I. Y. (2001, January). Iron cycling and
992 nutrient-limitation patterns in surface waters of the World Ocean. *Deep Sea Research*
993 *Part II: Topical Studies in Oceanography*, 49(1-3), 463–507. Retrieved 2023-07-25,
994 from <https://linkinghub.elsevier.com/retrieve/pii/S0967064501001096> doi:
995 10.1016/S0967-0645(01)00109-6
- 996 Nisancioglu, K. H., Raymo, M. E., & Stone, P. H. (2003, March). Reorganization of
997 Miocene deep water circulation in response to the shoaling of the Central American
998 Seaway: REORGANIZATION OF MIOCENE DEEP WATER CIRCULATION. *Pa-
999 leoceanography*, 18(1), n/a–n/a. Retrieved 2021-05-10, from [http://doi.wiley.com/](http://doi.wiley.com/10.1029/2002PA000767)
1000 [10.1029/2002PA000767](http://doi.wiley.com/10.1029/2002PA000767) doi: 10.1029/2002PA000767
- 1001 O’Dea, A., Lessios, H. A., Coates, A. G., Eytan, R. I., Restrepo-Moreno, S. A., Cione, A. L.,
1002 ... Jackson, J. B. C. (2016, August). Formation of the Isthmus of Panama. *Science*
1003 *Advances*, 2(8), e1600883. Retrieved 2022-09-22, from [https://www.science.org/](https://www.science.org/doi/10.1126/sciadv.1600883)
1004 [doi/10.1126/sciadv.1600883](https://www.science.org/doi/10.1126/sciadv.1600883) doi: 10.1126/sciadv.1600883
- 1005 Pillot, Q. (2022). *IPSL-CM5A2 source code used for "Evolution of ocean circulation in*
1006 *the North Atlantic Ocean during the Miocene: impact of the Greenland Ice Sheet and*
1007 *the Eastern Tethys Seaway". Zenodo. Retrieved from [https://doi.org/10.5281/](https://doi.org/10.5281/zenodo.6772699)
1008 [zenodo.6772699](https://doi.org/10.5281/zenodo.6772699) ([Software]) doi: 10.5281/zenodo.6772699*
- 1009 Pillot, Q. (2023). *Data For "Impact of dust and temperature on primary productivity in*
1010 *Late Miocene oceans". Zenodo. Retrieved from <https://doi.org/10.5281/zenodo>*

- 1011 .10407477 ([Dataset]) doi: 10.5281/zenodo.10407476
- 1012 Pillot, Q., Donnadieu, Y., Sarr, A.-C., Ladant, J.-B., & Suchéras-Marx, B. (2022).
 1013 Evolution of Ocean Circulation in the North Atlantic Ocean During the Miocene:
 1014 Impact of the Greenland Ice Sheet and the Eastern Tethys Seaway. *Paleoceanog-*
 1015 *raphy and Paleoclimatology*, 37(8), e2022PA004415. Retrieved 2022-09-07, from
 1016 <http://onlinelibrary.wiley.com/doi/abs/10.1029/2022PA004415> (eprint:
 1017 <https://agupubs.onlinelibrary.wiley.com/doi/pdf/10.1029/2022PA004415>) doi: 10
 1018 .1029/2022PA004415
- 1019 Pillot, Q., Suchéras-Marx, B., Sarr, A.-C., Bolton, C. T., & Donnadieu, Y.
 1020 (2023). A Global Reassessment of the Spatial and Temporal Expres-
 1021 sion of the Late Miocene Biogenic Bloom. *Paleoceanography and Paleo-*
 1022 *climatology*, 38(3), e2022PA004564. Retrieved 2023-03-30, from [https://](https://onlinelibrary.wiley.com/doi/abs/10.1029/2022PA004564)
 1023 onlinelibrary.wiley.com/doi/abs/10.1029/2022PA004564 (eprint:
 1024 <https://agupubs.onlinelibrary.wiley.com/doi/pdf/10.1029/2022PA004564>) doi:
 1025 10.1029/2022PA004564
- 1026 Pisias, N., Mayer, L., Janecek, T., Palmer-Julson, A., & van Andel, T. (Eds.). (1995).
 1027 *Proceedings of the Ocean Drilling Program, 138 Scientific Results* (Vol. 138).
 1028 Ocean Drilling Program. Retrieved 2020-12-15, from [http://www-odp.tamu.edu/](http://www-odp.tamu.edu/publications/138_SR/138TOC.HTM)
 1029 [publications/138_SR/138TOC.HTM](http://www-odp.tamu.edu/publications/138_SR/138TOC.HTM) doi: 10.2973/odp.proc.sr.138.1995
- 1030 Polissar, P. J., Rose, C., Uno, K. T., Phelps, S. R., & deMenocal, P. (2019, August).
 1031 Synchronous rise of African C4 ecosystems 10 million years ago in the absence of arid-
 1032 ification. *Nature Geoscience*, 12(8), 657–660. Retrieved 2023-07-26, from [https://](https://www.nature.com/articles/s41561-019-0399-2)
 1033 www.nature.com/articles/s41561-019-0399-2 doi: 10.1038/s41561-019-0399-2
- 1034 Poore, H. R., Samworth, R., White, N. J., Jones, S. M., & McCave, I. N. (2006, June). Neo-
 1035 gene overflow of Northern Component Water at the Greenland-Scotland Ridge: NEO-
 1036 GENE OVERFLOW OF NCW. *Geochemistry, Geophysics, Geosystems*, 7(6), n/a-
 1037 n/a. Retrieved 2020-08-28, from <http://doi.wiley.com/10.1029/2005GC001085>
 1038 doi: 10.1029/2005GC001085
- 1039 Pound, M. J., Haywood, A. M., Salzmann, U., & Riding, J. B. (2012, April). Global vegeta-
 1040 tion dynamics and latitudinal temperature gradients during the Mid to Late Miocene
 1041 (15.97–5.33Ma). *Earth-Science Reviews*, 112(1-2), 1–22. Retrieved 2022-07-04,
 1042 from <https://linkinghub.elsevier.com/retrieve/pii/S0012825212000165> doi:
 1043 10.1016/j.earscirev.2012.02.005
- 1044 Rae, J. W., Zhang, Y. G., Liu, X., Foster, G. L., Stoll, H. M., & Whiteford, R. D.
 1045 (2021, May). Atmospheric CO₂ over the Past 66 Million Years from Marine
 1046 Archives. *Annual Review of Earth and Planetary Sciences*, 49(1), 609–641. Re-
 1047 trieved 2021-09-01, from [https://www.annualreviews.org/doi/10.1146/annurev](https://www.annualreviews.org/doi/10.1146/annurev-earth-082420-063026)
 1048 [-earth-082420-063026](https://www.annualreviews.org/doi/10.1146/annurev-earth-082420-063026) doi: 10.1146/annurev-earth-082420-063026
- 1049 Rech, J. A., Currie, B. S., Jordan, T. E., Riquelme, R., Lehmann, S. B., Kirk-Lawlor,
 1050 N. E., ... Gooley, J. T. (2019, January). Massive middle Miocene gypsic paleosols
 1051 in the Atacama Desert and the formation of the Central Andean rain-shadow. *Earth*
 1052 *and Planetary Science Letters*, 506, 184–194. Retrieved 2023-08-18, from [https://](https://linkinghub.elsevier.com/retrieve/pii/S0012821X18306423)
 1053 linkinghub.elsevier.com/retrieve/pii/S0012821X18306423 doi: 10.1016/j.epsl
 1054 .2018.10.040
- 1055 Sarmiento, J. L., Gruber, N., Brzezinski, M. A., & Dunne, J. P. (2004, January). High-
 1056 latitude controls of thermocline nutrients and low latitude biological productivity.
 1057 *Nature*, 427(6969), 56–60. Retrieved 2023-07-27, from [https://www.nature.com/](https://www.nature.com/articles/nature02127)
 1058 [articles/nature02127](https://www.nature.com/articles/nature02127) doi: 10.1038/nature02127
- 1059 Sarr, A.-C., Donnadieu, Y., Bolton, C. T., Ladant, J.-B., Licht, A., Fluteau, F., ... Dupont-
 1060 Nivet, G. (2022, April). Neogene South Asian monsoon rainfall and wind histories
 1061 diverged due to topographic effects. *Nature Geoscience*, 15(4), 314–319. Retrieved
 1062 2022-06-22, from <https://www.nature.com/articles/s41561-022-00919-0> doi:
 1063 10.1038/s41561-022-00919-0
- 1064 Schneider, B., & Schmittner, A. (2006, June). Simulating the impact of the Pana-
 1065 manian seaway closure on ocean circulation, marine productivity and nutrient cy-

- 1066 cling. *Earth and Planetary Science Letters*, *246*(3-4), 367–380. Retrieved 2021-10-28,
1067 from <https://linkinghub.elsevier.com/retrieve/pii/S0012821X0600330X> doi:
1068 10.1016/j.epsl.2006.04.028
- 1069 Schuster, M., Düringer, P., Ghienne, J.-F., Vignaud, P., Mackaye, H. T., Likius, A., &
1070 Brunet, M. (2006, February). The Age of the Sahara Desert. *Science*, *311*(5762), 821–
1071 821. Retrieved 2022-07-19, from [https://www.science.org/doi/10.1126/science](https://www.science.org/doi/10.1126/science.1120161)
1072 .1120161 doi: 10.1126/science.1120161
- 1073 Sepulchre, P., Arsouze, T., Donnadiou, Y., Dutay, J.-C., Jaramillo, C., Le Bras, J., ...
1074 Waite, A. J. (2014, March). Consequences of shoaling of the Central American
1075 Seaway determined from modeling Nd isotopes. *Paleoceanography*, *29*(3), 176–189.
1076 Retrieved 2021-05-10, from <http://doi.wiley.com/10.1002/2013PA002501> doi:
1077 10.1002/2013PA002501
- 1078 Sepulchre, P., Caubel, A., Ladant, J.-B., Bopp, L., Boucher, O., Braconnot, P., ... Tardif,
1079 D. (2020, July). IPSL-CM5A2 – an Earth system model designed for multi-millennial
1080 climate simulations. *Geoscientific Model Development*, *13*(7), 3011–3053. Retrieved
1081 2022-01-03, from <https://gmd.copernicus.org/articles/13/3011/2020/> doi: 10
1082 .5194/gmd-13-3011-2020
- 1083 Sepulchre, P., Ramstein, G., Fluteau, F., Schuster, M., Tiercelin, J.-J., & Brunet, M. (2006,
1084 September). Tectonic Uplift and Eastern Africa Aridification. *Science*, *313*(5792),
1085 1419–1423. Retrieved 2023-08-04, from [https://www.science.org/doi/10.1126/](https://www.science.org/doi/10.1126/science.1129158)
1086 *science.1129158* doi: 10.1126/science.1129158
- 1087 Sharples, J., Middelburg, J. J., Fennel, K., & Jickells, T. D. (2017). What
1088 proportion of riverine nutrients reaches the open ocean? *Global Bio-*
1089 *geochemical Cycles*, *31*(1), 39–58. Retrieved 2023-07-27, from [https://](https://onlinelibrary.wiley.com/doi/abs/10.1002/2016GB005483)
1090 onlinelibrary.wiley.com/doi/abs/10.1002/2016GB005483 (eprint:
1091 <https://agupubs.onlinelibrary.wiley.com/doi/pdf/10.1002/2016GB005483>) doi:
1092 10.1002/2016GB005483
- 1093 Shi, J.-H., Gao, H.-W., Zhang, J., Tan, S.-C., Ren, J.-L., Liu, C.-G., ... Yao,
1094 X. (2012). Examination of causative link between a spring bloom and
1095 dry/wet deposition of Asian dust in the Yellow Sea, China. *Journal of*
1096 *Geophysical Research: Atmospheres*, *117*(D17). Retrieved 2023-07-27, from
1097 <https://onlinelibrary.wiley.com/doi/abs/10.1029/2012JD017983> (eprint:
1098 <https://onlinelibrary.wiley.com/doi/pdf/10.1029/2012JD017983>) doi: 10.1029/
1099 2012JD017983
- 1100 Sosdian, S. M., Greenop, R., Hain, M. P., Foster, G. L., Pearson, P. N., & Lear, C. H. (2018,
1101 September). Constraining the evolution of Neogene ocean carbonate chemistry using
1102 the boron isotope pH proxy. *Earth and Planetary Science Letters*, *498*, 362–376. Re-
1103 trieved 2021-09-01, from [https://www.sciencedirect.com/science/article/pii/](https://www.sciencedirect.com/science/article/pii/S0012821X1830356X)
1104 S0012821X1830356X doi: 10.1016/j.epsl.2018.06.017
- 1105 Steinacher, M., Joos, F., Frölicher, T. L., Bopp, L., Cadule, P., Cocco, V., ... Segschnei-
1106 der, J. (2010, March). Projected 21st century decrease in marine productivity: a
1107 multi-model analysis. *Biogeosciences*, *7*(3), 979–1005. Retrieved 2023-08-08, from
1108 <https://bg.copernicus.org/articles/7/979/2010/bg-7-979-2010.html> (Pub-
1109 lisher: Copernicus GmbH) doi: 10.5194/bg-7-979-2010
- 1110 Steinthorsdottir, M., Coxall, H. K., de Boer, A. M., Huber, M., Barbolini, N., Brad-
1111 shaw, C. D., ... Strömberg, C. A. E. (2021, April). The Miocene: The Fu-
1112 ture of the Past. *Paleoceanography and Paleoclimatology*, *36*(4). Retrieved 2021-
1113 05-06, from <https://onlinelibrary.wiley.com/doi/10.1029/2020PA004037> doi:
1114 10.1029/2020PA004037
- 1115 Tagliabue, A., Bopp, L., & Aumont, O. (2008, January). Ocean biogeochemistry exhibits
1116 contrasting responses to a large scale reduction in dust deposition. *Biogeosciences*,
1117 *5*(1), 11–24. Retrieved 2023-06-28, from [https://bg.copernicus.org/articles/5/](https://bg.copernicus.org/articles/5/11/2008/bg-5-11-2008.html)
1118 11/2008/bg-5-11-2008.html (Publisher: Copernicus GmbH) doi: 10.5194/bg-5-11
1119 -2008
- 1120 Tagliabue, A., Bopp, L., & Aumont, O. (2009). Evaluating the importance

- 1121 of atmospheric and sedimentary iron sources to Southern Ocean biogeochem-
 1122 istry. *Geophysical Research Letters*, 36(13). Retrieved 2023-06-28, from
 1123 <https://onlinelibrary.wiley.com/doi/abs/10.1029/2009GL038914> (_eprint:
 1124 <https://agupubs.onlinelibrary.wiley.com/doi/pdf/10.1029/2009GL038914>) doi: 10
 1125 .1029/2009GL038914
- 1126 Tan, N., Zhang, Z. S., Guo, Z. T., Guo, C. C., Zhang, Z. J., He, Z. L., & Ramstein, G. (2022).
 1127 Recognizing the Role of Tropical Seaways in Modulating the Pacific Circulation.
 1128 *Geophysical Research Letters*, 49(19), e2022GL099674. Retrieved 2023-08-18, from
 1129 <https://onlinelibrary.wiley.com/doi/abs/10.1029/2022GL099674> (_eprint:
 1130 <https://agupubs.onlinelibrary.wiley.com/doi/pdf/10.1029/2022GL099674>) doi: 10
 1131 .1029/2022GL099674
- 1132 Tardif, D., Sarr, A.-C., Fluteau, F., Licht, A., Kaya, M., Ladant, J.-B., ... Banfield,
 1133 W. (2023, August). The role of paleogeography in Asian monsoon evolution:
 1134 a review and new insights from climate modelling. *Earth-Science Reviews*, 243,
 1135 104464. Retrieved 2023-08-04, from [https://linkinghub.elsevier.com/retrieve/
 1136 pii/S0012825223001538](https://linkinghub.elsevier.com/retrieve/pii/S0012825223001538) doi: 10.1016/j.earscirev.2023.104464
- 1137 Tardif, D., Toumoulin, A., Fluteau, F., Donnadiou, Y., Le Hir, G., Barbolini, N., ...
 1138 Dupont-Nivet, G. (2021, October). Orbital variations as a major driver of climate
 1139 and biome distribution during the greenhouse to icehouse transition. *Science Ad-
 1140 vances*, 7(43), eabh2819. Retrieved 2023-09-06, from [https://www.science.org/
 1141 doi/10.1126/sciadv.abh2819](https://www.science.org/doi/10.1126/sciadv.abh2819) doi: 10.1126/sciadv.abh2819
- 1142 Tauxe, L., & Feakins, S. J. (2020). A Reassessment of the Chronostratig-
 1143 raphy of Late Miocene C3-C4 Transitions. *Paleoceanography and Paleo-
 1144 climatology*, 35(7), e2020PA003857. Retrieved 2022-07-19, from [http://
 1145 onlinelibrary.wiley.com/doi/abs/10.1029/2020PA003857](http://onlinelibrary.wiley.com/doi/abs/10.1029/2020PA003857) (_eprint:
 1146 <https://agupubs.onlinelibrary.wiley.com/doi/pdf/10.1029/2020PA003857>) doi:
 1147 10.1029/2020PA003857
- 1148 Valcke, S. (2013, March). The OASIS3 coupler: a European climate modelling community
 1149 software. *Geoscientific Model Development*, 6(2), 373–388. Retrieved 2022-01-03,
 1150 from <https://gmd.copernicus.org/articles/6/373/2013/> doi: 10.5194/gmd-6
 1151 -373-2013
- 1152 Wang, C., Dai, J., Zhao, X., Li, Y., Graham, S. A., He, D., ... Meng, J. (2014, May).
 1153 Outward-growth of the Tibetan Plateau during the Cenozoic: A review. *Tectono-
 1154 physics*, 621, 1–43. Retrieved 2022-07-06, from [https://linkinghub.elsevier.com/
 1155 retrieve/pii/S0040195114000729](https://linkinghub.elsevier.com/retrieve/pii/S0040195114000729) doi: 10.1016/j.tecto.2014.01.036
- 1156 Wright, J. D., & Miller, K. G. (1996). Control of North Atlantic Deep Water Circula-
 1157 tion by the Greenland-Scotland Ridge. *Paleoceanography*, 11(2), 157–170. Retrieved
 1158 2022-07-06, from <http://onlinelibrary.wiley.com/doi/abs/10.1029/95PA03696>
 1159 (_eprint: <https://agupubs.onlinelibrary.wiley.com/doi/pdf/10.1029/95PA03696>) doi:
 1160 10.1029/95PA03696
- 1161 Yang, R., Yang, Y., Fang, X., Ruan, X., Galy, A., Ye, C., ... Han, W. (2019). Late Miocene
 1162 Intensified Tectonic Uplift and Climatic Aridification on the Northeastern Tibetan
 1163 Plateau: Evidence From Clay Mineralogical and Geochemical Records in the Xin-
 1164 ing Basin. *Geochemistry, Geophysics, Geosystems*, 20(2), 829–851. Retrieved 2022-
 1165 07-20, from <http://onlinelibrary.wiley.com/doi/abs/10.1029/2018GC007917>
 1166 (_eprint: <https://agupubs.onlinelibrary.wiley.com/doi/pdf/10.1029/2018GC007917>)
 1167 doi: 10.1029/2018GC007917
- 1168 Zhang, L., Chen, M., Xiang, R., Zhang, L., & Lu, J. (2009, June). Productiv-
 1169 ity and continental denudation history from the South China Sea since the late
 1170 Miocene. *Marine Micropaleontology*, 72(1-2), 76–85. Retrieved 2020-11-09, from
 1171 <https://linkinghub.elsevier.com/retrieve/pii/S0377839809000383> doi: 10
 1172 .1016/j.marmicro.2009.03.006
- 1173 Zhang, Z., Ramstein, G., Schuster, M., Li, C., Contoux, C., & Yan, Q. (2014, Septem-
 1174 ber). Aridification of the Sahara desert caused by Tethys Sea shrinkage during the
 1175 Late Miocene. *Nature*, 513(7518), 401–404. Retrieved 2022-09-22, from <http://>

